2007-12-07

Solid Phase Crystallization of Vanadium Dioxide Thin Films and Characterization Through Scanning Electron Microscopy

Felipe Rivera
Brigham Young University - Provo

SOLID PHASE CRYSTALLIZATION OF VANADIUM DIOXIDE THIN FILMS AND

CHARACTERIZATION THROUGH SCANNING ELECTRON MICROSCOPY

by

Felipe Rivera

A thesis submitted to the faculty of

Brigham Young University

in partial fulfillment of the requirements for the degree of

Master of Science

Department of Physics and Astronomy

Brigham Young University

December 2007

BRIGHAM YOUNG UNIVERSITY

GRADUATE COMMITTEE APPROVAL

of a thesis submitted by

Felipe Rivera

This thesis has been read by each member of the following graduate committee and by majority vote has been found to be satisfactory.

_____   _____

Date   Richard R. Vanfleet, Chair

_____   _____

Date   Robert C. Davis

_____   _____

Date   Branton J. Campbell

BRIGHAM YOUNG UNIVERSITY

As chair of the candidate's graduate committee, I have read the thesis of Felipe Rivera in its final form and have found that (1) its format, citations, and bibliographical style are consistent and acceptable and fulfill university and department style requirements; (2) its illustrative materials including figures, tables, and charts are in place; and (3) the final manuscript is satisfactory to the graduate committee and is ready for submission to the university library.

_____   _____
Date   Richard R. Vanfleet
                                 Chair, Graduate Committee

Accepted for the Department

                                 _____
                                 Ross L. Spencer, Chair
                                 Department of Physics and Astronomy

Accepted for the College

                                 _____
                                 Thomas W. Sederberg, Associate Dean
                                 The College of Physical and Mathematical Sciences

SOLID PHASE CRYSTALLIZATION OF VANADIUM DIOXIDE THIN FILMS AND

CHARACTERIZATION THROUGH SCANNING ELECTRON MICROSCOPY

Felipe Rivera

Department of Physics and Astronomy

Master of Science

ABSTRACT

Crystalline films of vanadium dioxide were obtained through thermal annealing of amorphous vanadium dioxide thin films sputtered on silicon dioxide. An annealing process was found that yielded polycrystalline vanadium dioxide thin films, semi-continuous thin films, and films of isolated single-crystal particles. Orientation Imaging Microscopy (OIM) was used to characterize and study the phase and the orientation of the vanadium dioxide crystals obtained, as well as to differentiate them from other vanadium oxide stoichiometries that may have formed during the annealing process. There was no evidence of any other vanadium oxides present in the prepared samples. Indexing of the crystals for the orientation study was performed with the Kikuchi patterns for the tetragonal phase of vanadium dioxide, since it was observed that the Kikuchi patterns for the monoclinic and tetragonal phases of vanadium dioxide are indistinguishable by OIM. It was found that a particle size of 100 nm was

in the lower limit of particles that could be reliably characterized with this technique. It was also found that all VO_2 crystals large enough to be indexed by OIM had a preferred orientation with the C axis of the tetragonal phase parallel to the plane of the specimen.

ACKNOWLEDGMENTS

undergraduate students to whom I am indebted, namely: Laurel Burk, from the University of Nebraska at Lincoln; Michael Miller, from the University of California, Los Angeles; and Brady Cox, from Brigham Young University. All of whom took the time to learn the intricacies of Electron Microscopy, and as a consequence allowed me to learn a from their successes and struggles. I would further like to thank Michael Clemens and Hiram Conley both of whom were invaluable assets in performing Atomic Force Microscope electrical measurements. The help obtained from many of these wonderful students would not have been possible without the funding provided by the NSF-REU program in the Physics and Astronomy Department at BYU. Most of all, I would like to thank my beloved and beautiful wife, Nancy Rivera, for her encouragement which empowered me to pursue graduate education, and for her formidable patience, love, and continuing reassurance these years. Also my children, Felipe, Cassandra, and Carolina, who, unknowingly, gave me that extra drive to complete this work. And to my parents, who have constantly supported, encouraged, and motivated me. Though I cannot name every single person that has given me their support, I would like to extend my gratitude to my relatives and friends who have also given me of their support.

Contents

List of Figures

List of Tables

Chapter 1

Introduction

Vanadium is a transition metal whose oxides undergo a metal-to-insulator transition (MIT)[1] at some characteristic temperature. [1,2] Among vanadium's oxides, vanadium dioxide (VO_2) has been extensively studied because its transition temperature occurs near room temperature (340K 68°C). [2–4] In single crystals, vanadium dioxide undergoes significant, abrupt, and reversible changes in several of its properties during its phase transition. These changes to its properties include: 1) A structural change from a low temperature semi-conducting monoclinic phase to a high-temperature tetragonal metallic phase; 2) a resistivity change of several orders of magnitude; and 3) a sharp change in optical transmittance in the infrared region. These optical and electronic properties that vanadium dioxide exhibits due to its phase transition hint at the use of this material for optical [5–9] and electronic [10,11] applications, such as thermochromic coatings for windows, fast optical and electronic switches, or thermal sensors.

---

[1]Also referred to as a semiconductor-to-metal transition (SMT)

1.1   Previous Work Done on Vanadium Dioxide

Several transition metal oxides form a wide range of materials in which to explore interesting physical phenomena. Some of these oxides exhibit phase transitions and varied electronic behavior that are widely observed in condensed matter physics [1,12]. Vanadium is one of such transition metals that has several oxides that undergo a metal-to-insulator transition (MIT) at some characteristic temperature. [1, 12, 13]

Vanadium dioxide (VO_2) has been a material of particular interest since the observation of its phase transition by F. Morin in 1959. [1] In his paper, Morin reported the conductivity and phase transitions for VO, VO_2, V_2O_3 and two other transition metal oxides. The reported change in conductivity during the transition for VO_2 is not as dramatic as that for VO or V_2O_3. However, VO_2 still exhibits a change of several orders of magnitude.[2] Furthermore, one of the compelling aspects that makes vanadium dioxide (VO_2) interesting to study (over the other vanadium oxide stoichiometries) is the temperature of its transition. 68^oC is a temperature easy to achieve, and this allows the use of many probing techniques to study the material as the transition takes place.

Several transition metal oxides show metallic properties. These properties have been modeled and are are often attributed to the 3d electron orbitals forming a narrow conductive band. [1] However, in the case of vanadium dioxide, and despite the work that has been done on this material, the nature of the phase transition still is very much debated. [3, 14–18]

---

[2]Figure 1.1 summarizes some of the results obtained by Morin as well as other results obtained by Kachi.

1.1.1 Some Known Vanadium Oxides

Vanadium has many varied valence states. Thus the synthesis of vanadium dioxide is a non trivial matter since the valence states of vanadium allow it to have various oxide stoichiometries all with different properties. Even when vanadium may be found in a single valence state in oxides such as VO, V_2O_3, VO_2 and V_2O_5 (Where the valence state is V^{2+}, V^{3+}, V^{4+}, and V^{5+} respectively) [12], a wide variety of mixed valence oxides also exist. [12, 13] Interestingly enough, the vanadium to oxygen ratio affects the structure and the properties of the material greatly. For example, C. Hébert reports that, "VO is a metal with rock-salt structure. V_2O_3 is in a paramagnetic metallic phase with corundum structure (α- Al_2O_3) above 165 K and an antiferromagnetic insulator with monoclinic structure below 165 K. VO_2 undergoes a first order transition from a diamagnetic semiconductor phase below 340 K to a paramagnetic metallic state with rutile structure above 340 K. V_2O_5 is a diamagnetic insulator at room temperature with orthorhombic structure." [12]

The change in conductivity was first used to study the phase transition in different materials. Thus, the conductivity of various vanadium oxides have been studied since the initial report performed by Morin in 1959. It was observed that slight deviations in the vanadium to oxygen ratio greatly changed the properties of the material. In addition to the vanadium oxides studies by Morin in 1959, Sujeki Kachi performed a study in 1963 on the electrical conductivity of V_2O_3, V_3O_5, V_4O_7, V_5O_9, V_6O_{11}, V_7O_{13}, V_2O_4, V_6O_{13}, and V_2O_5. These stoichiometries are slight variations in the vanadium to oxygen ratio, yet their electrical properties are remarkably different. Figure 1.1 qualitatively summarizes the differences in electrical conductivity found in the studies performed by Morin (1959) and Kachi (1963). [1, 13] The figure shows eleven vanadium oxides with stoichiometries that vary from a 2:2 vanadium to oxygen ratio (VO) to a 2:5 vanadium to oxygen ratio (V_2O_5). Phase transitions are evident
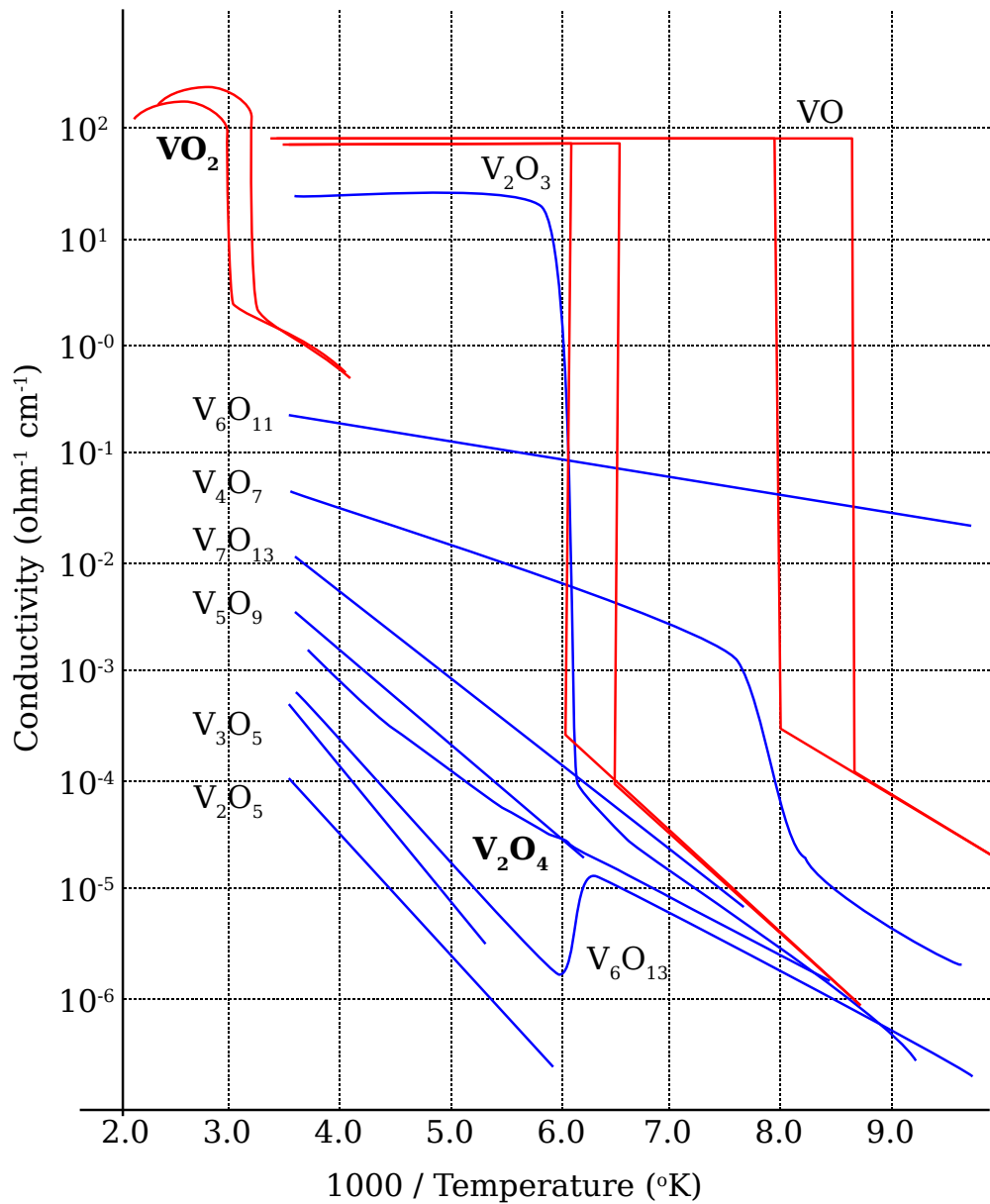
Figure 1.1 Conductivity as a function of reciprocal temperature for varied vanadium oxides, including V_2O_3, V_3O_5, V_4O_7, V_5O_9, V_6O_{11}, V_7O_{13}, V_2O_4, V_6O_{13}, and V_2O_5. [1, 13]. These conductivities were reported in 1959 by Morin (in red) and in 1963 by Kachi. Notice there is an entry for VO_2 reported by Morin and one for V_2O_4 as reported by Kachi. Though the phase transition for VO_2 is not as dramatic as the transitions for VO or V_2O_3, it still exhibits a conductivity change several orders of magnitude.

Material	$a1$ (Å)	$a2$ (Å)	$a3$ (Å)	α	β	γ
VO	4.120	4.120	4.120	90.0	90.0	90.0
V_2O_3	4.978	4.978	13.965	90.0	90.0	120.0
VO_2	5.753	4.526	5.383	90.0	122.6	90.0
V_2O_5	10.011	3.564	4.368	90.0	90.0	90.0

Table 1.1 Lattice Parameters for known crystal structures of several vanadium oxides. The vanadium dioxide structure stated for VO_2 is the room temperature monoclinic structure. [22]

for VO, V_2O_3, and VO_2.

Variations in the oxidation states of vanadium not only have an effect in the electrical conductivity of the material, as figure 1.1 qualitatively shows, but these materials also exhibit different magnetic properties, and some (not all) do show metal to insulator transitions. [13, 19–21]

VO_x Structural Models

Another aspect that distinguished between several of the known vanadium oxides is their crystal structure. Table 1.1 shows the different lattice parameters between different stoichiometries in vanadium oxides. Some of these differences can be observed in the diagrams of their crystal structures show in in figure 1.2.

The synthesis of vanadium dioxide is non-trivial due to the many oxides possible. However (to our benefit) the remarked distinctions (structurally and electrically) between the various oxides help to determine the quality of the material produced by a specific process.
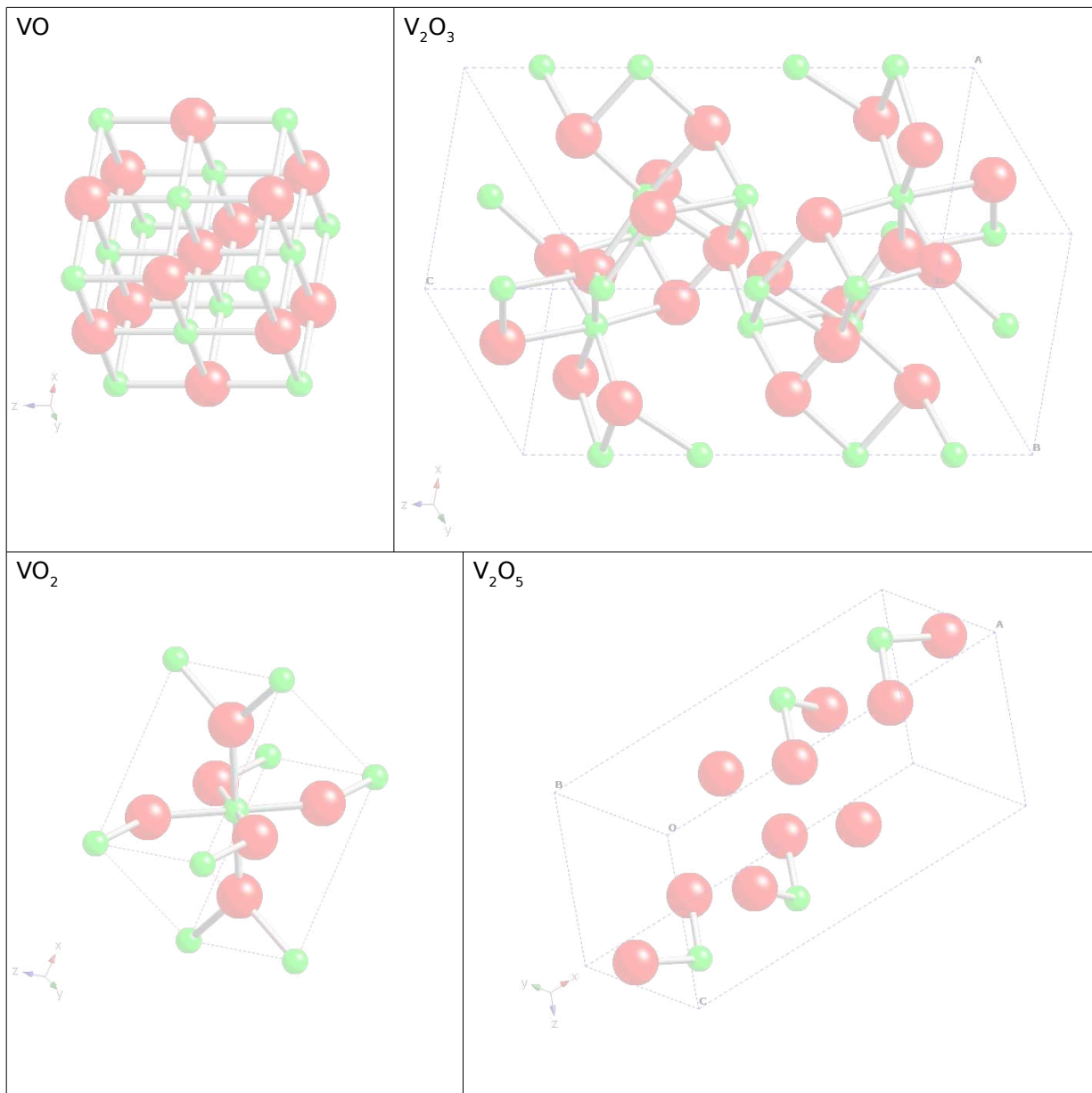
Figure 1.2 Crystal Structures for VO, V_2O_3, VO_2, and V_2O_5. The vanadium dioxide structure modeled corresponds to the high temperature tetragonal structure. [22] Changes in the vanadium to oxygen ratio affect the crystal structure.

1.1.2 Properties Specific to Vanadium Dioxide

As mentioned in the previous section, the synthesis of high-quality vanadium dioxide is not a trivial matter due to the many oxidation states available for vanadium. Nonetheless, different methods have been used to successfully produce high-quality vanadium dioxide thin films[3]. [4] The quality of these deposited films has been determined by examining some of the properties that are characteristic of vanadium dioxide such as conductivity, IR transmittance/reflectance, crystal structure, transition temperature[4], and others. [1, 5, 6, 10, 11, 11, 23–26]

Structural Change During the Phase Transition

In single crystals, vanadium dioxide (VO_2) undergoes a structural phase transition near 68°C. Structurally, VO_2 shifts between a low temperature low-symmetry monoclinic structure[5] to a high temperature, higher-symmetry tetragonal structure. [12, 23–25] Table 1.2 shows three of the documented structures for VO_2. The lattice parameters for these three structures were found in the Inorganic Crystal Structure Database (ICSD) [22]

Since the electronic band structure of a material is dependent on the crystal structure, a change in the crystal structure comes with a change in the band structure. These crystal structures have been studied and modeled in attempts to explain the nature of the transition. [3, 14, 15] The computational models show changes in the band

---

[3]See Section 1.2

[4]Naturally, a change in one of these properties at, or near, the transition temperature is often quoted as an indicator of the quality of the VO_2 crystals produced. Nevertheless, this is not always the case, sometimes, the crystal structure is used as the determining factor to determine the quality of the VO_2 crystals produced.

[5]The monoclinic structure of vanadium dioxide can be altered by other factors such as stress, and doping. However, this tetragonal structure seems to be well accepted.

Tetragonal T> 68°C	Monoclinic T< 68°C	Monoclinic Stressed T< 68°C
4.55350 Å $a1$	5.38250 Å $a3$	4.52550 Å $a3$
4.55350 Å $a2$	4.52630 Å $a2$	9.06640 Å $a1$
2.84940 Å $a3$	5.75290 Å $a1$	5.79700 Å $a2$
$\alpha = 90°$	$\beta = 122.8°$	$\gamma = 90°$
$\beta = 90°$	$\alpha = 90°$	$\alpha = 90°$
$\gamma = 90°$	$\gamma = 90°$	$\beta = 91.88°$

Table 1.2 Lattice Parameters from three known VO_2 crystal structures. [22] The order is such as to show the corresponding change in the lattice parameter as the transition takes place.

structure of VO_2 as the transition takes place.[6] Though the nature of the transition in VO_2 still is under debate, the theoretical studies have shed light on the band structure, Fermi levels, band gap, and electronic properties of the material. [3, 14, 15]

Nonetheless, the knowledge of the crystal structure allows for the use of scattering techniques (such as x-ray diffraction) to probe the transition of crystalline vanadium dioxide. [23–25, 27] Figures 1.3, 1.4, and 1.5 show some of the structural differences between three known phases in vanadium dioxide as seen from three different directions (100, 010, and 001 of the tetragonal phase respectively).[7] As seen from the figures, some of the differences are clear enough that scattering experiments might be used to observe the phase transition. [23, 24]

---

[6]Unfortunately, many of the computational models are unable to obtain a band gap at the Fermi level in the monoclinic structure. [15]

[7]A useful tool that helps model the phase transition is isodisplace. [28] See appendix B
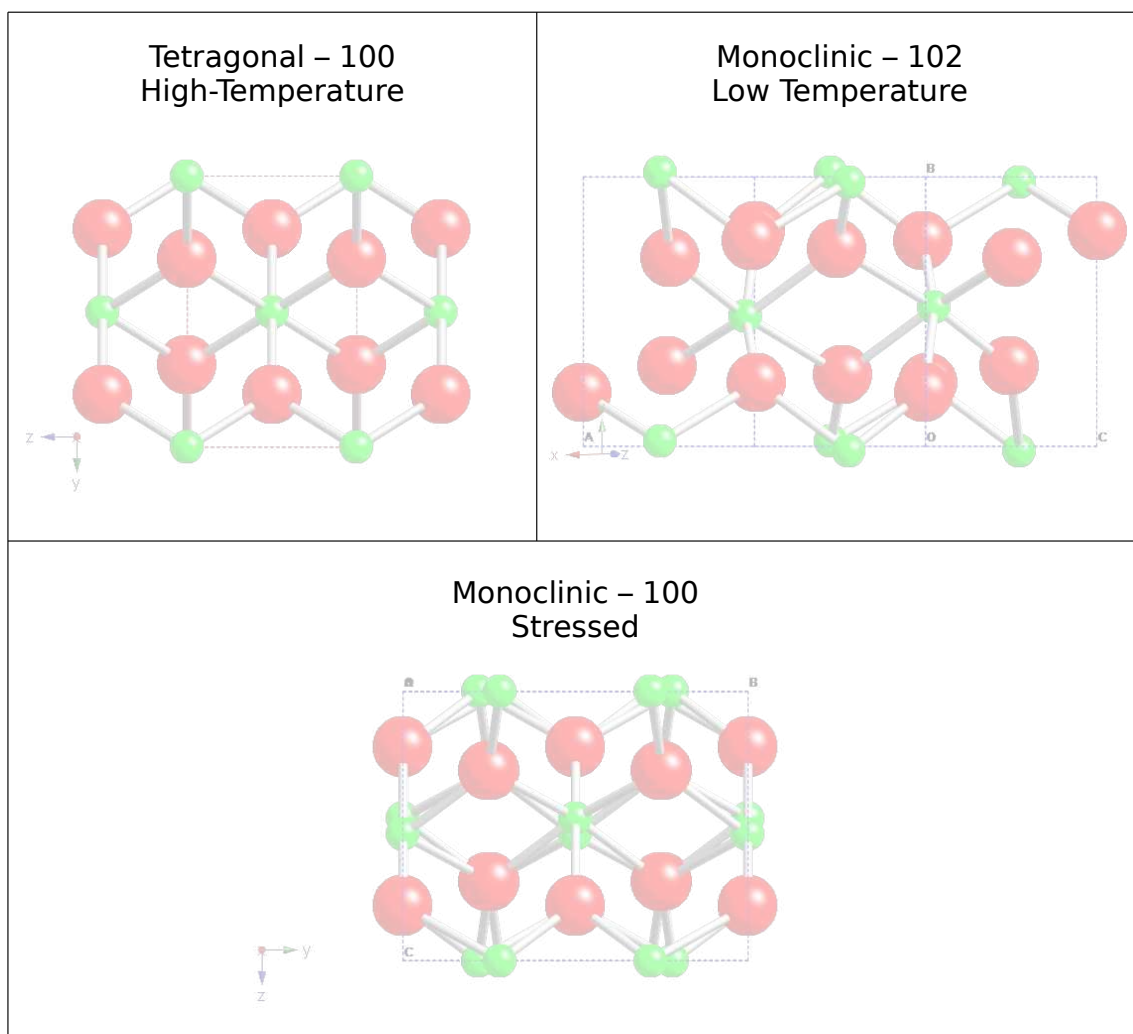
Figure 1.3 Comparison of three known vanadium dioxide structures. The monoclinic structures are oriented in such a way as to correspond with the 100 view of the tetragonal phase
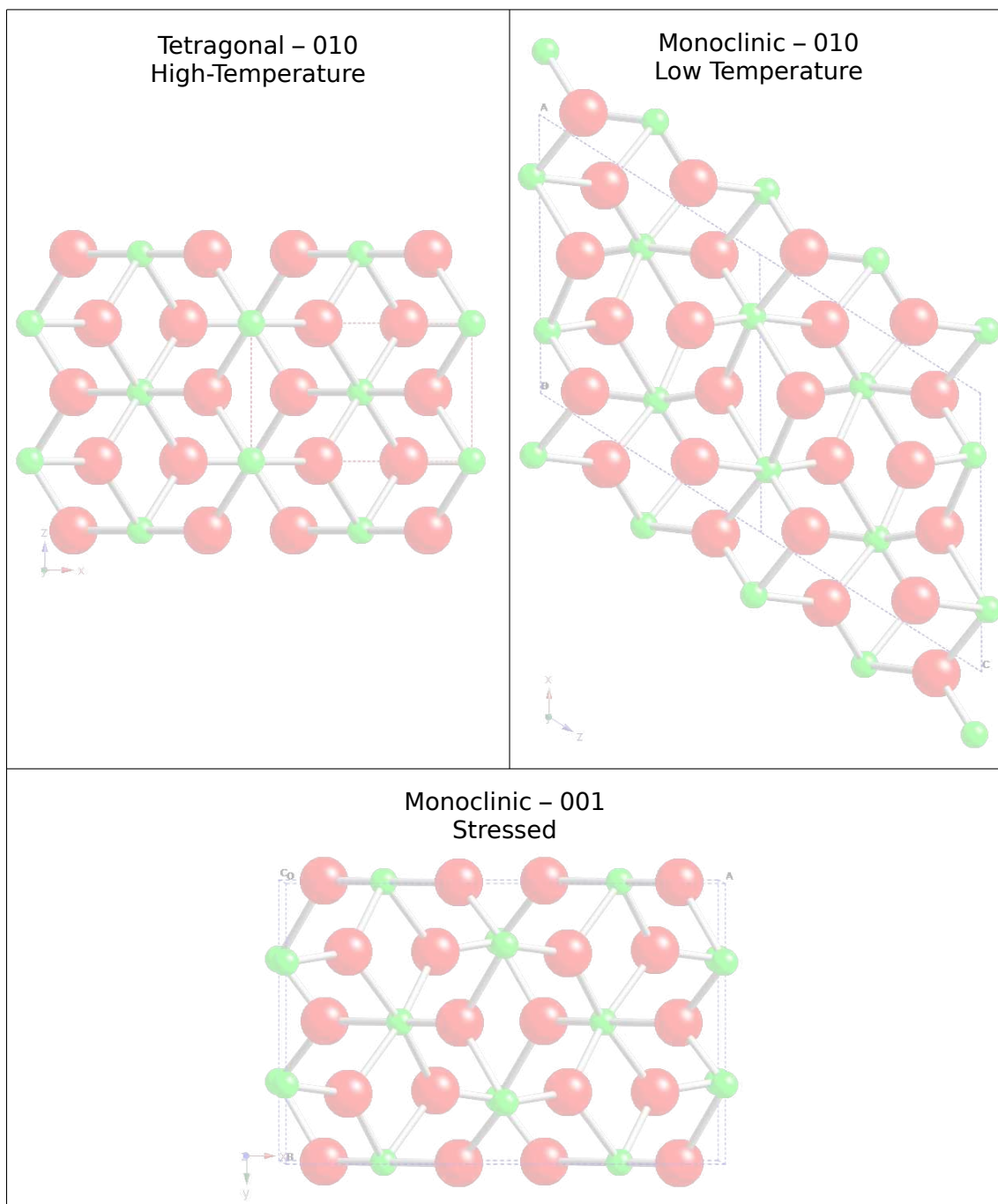
Figure 1.4 Comparison of three known vanadium dioxide structures. The monoclinic structures are oriented in such a way as to correspond with the 010 view of the tetragonal phase
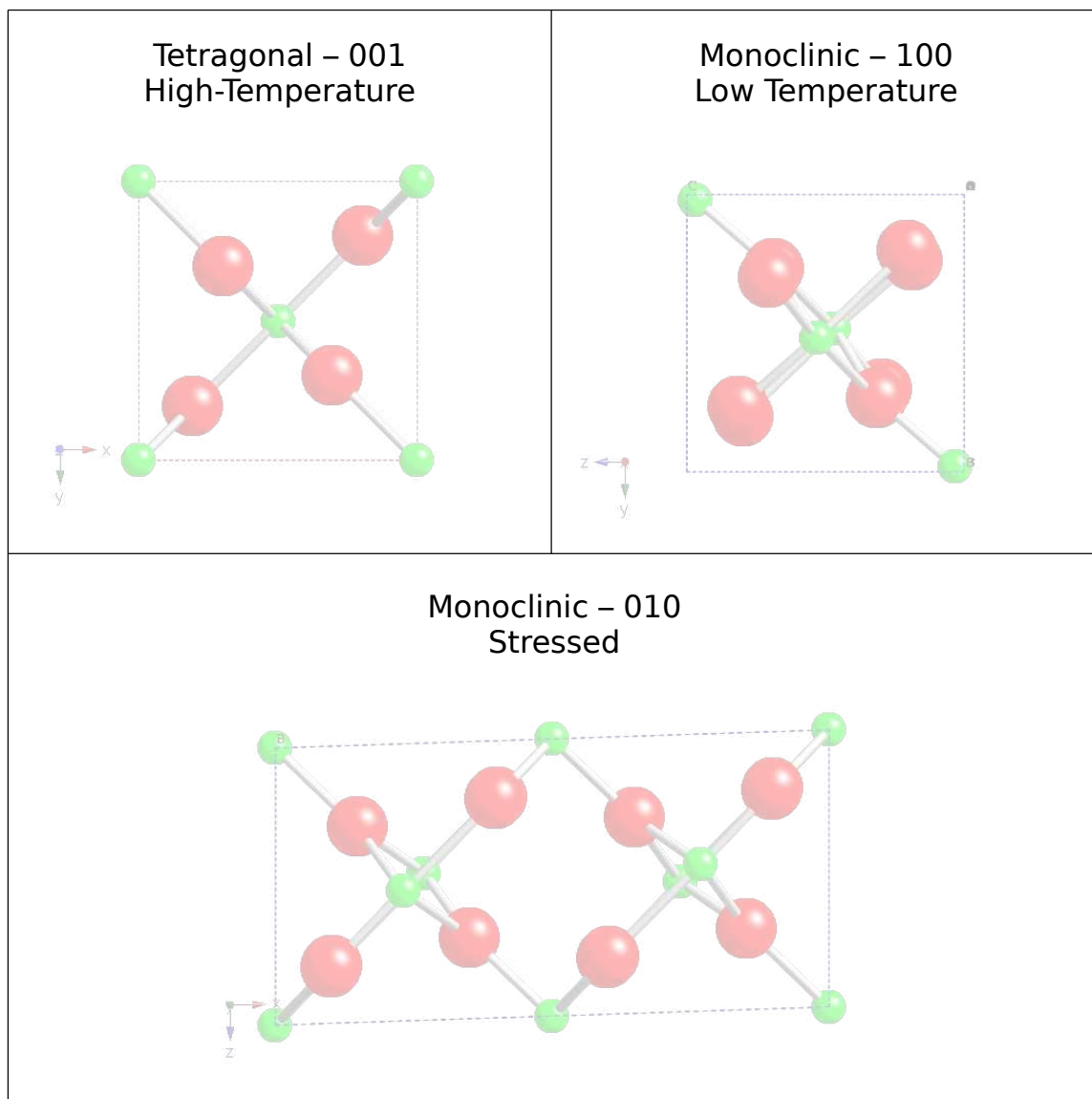
Figure 1.5 Comparison of three known vanadium dioxide structures. The monoclinic structures are oriented in such a way as to correspond with the 001 view of the tetragonal phase

Electrical Conductivity Change During the Phase Transition

The original observation where vanadium dioxide underwent a metal to insulator phase transition was done by electrical conductivity. [1] Below the 68°C transition temperature, crystalline VO_2 is found in a semiconducting phase. However, above the transition temperature crystalline vanadium dioxide exhibits a change in resistivity as high as 5 orders of magnitude[8]. [5, 10, 29] Though the change in electrical conductivity is a rather dramatic change easily observable, other electrical changes (such as a change in capacitance) may also be observed. [11]

Optical Change During the Phase Transition

The optical properties of vanadium dioxide began to be studied shortly after Morin's 1959 paper. H. W. Verleur reported in 1968 the optical transmission of a 100 nm polycrystalline thin film of VO_2 with photon energies from .25 eV to 5 eV. [5] This change in the relative transmittance of VO_2 thin films is more easily observed in the infrared region [6–9, 30–32], and has been used to study the hysteresis and speed of the transition. It is interesting to note, that this optical change during the phase transition of VO_2 has been timed to take place in the sub-pico second regime. [30, 32]

Methods Shown to Modulate or Induce the Phase Transition in VO_2

Even though the phase transition for vanadium dioxide is cited to be 68°C (it was first induced by temperature [1]) there are several factors that will modify, tune, alter, or even induce the phase transition. Variations in stoichiometry, particle size, stress, misorientations between grains, morphological faults, dopants, and other "imperfections" have been used qualitatively to describe changes in the transition temperature,

---

[8]Figure 1 shows an electrical conductivity change of 2 orders of magnitude. This difference is attributed to grain boundaries, percolation effects and polycrystallinity. [5, 10, 29]

hysteresis, and sharpness of the transition. [8, 26, 29, 31] Further, the phase transition in vanadium dioxide has also been induced by methods other than temperature. Some optical measurements have been performed using a pulse-probe technique to induce and time the phase transition. [30, 32] According to Cavalleri, the transition was induced by "prompt hole photo-doping." [30]

1.2   Common Deposition Methods for VO_2 Thin Films

Thin film deposition is an inexpensive method of integrating materials because there is no need to create large bulk samples and it is relatively easy to deposit and pattern onto a variety of substrates. In the case for vanadium dioxide, large single crystals have not been used technically as they fracture due to mechanical tensions that occur during the phase transition. Fortunately, these ruptures have not been observed in thin films. [11] As mentioned in previous sections, due to the many oxidation states available for vanadium, the synthesis of high-quality vanadium dioxide is not a trivial matter. Nonetheless, different methods have been used to successfully produce high-quality vanadium dioxide thin films on a variety of substrates. Though the deposition details vary from paper to paper in the literature, deposition methods include: RF and DC magnetron reactive sputtering, sol-gel deposition, reactive ion-beam sputtering, reactive evaporation, chemical vapor deposition (including chemical metal-organic vapor deposition) [4], pulsed laser deposition [33,34], ion implantation [35], and others. Since it is difficult to produce stoichiometric vanadium dioxide using these methods, often a post annealing process is used to produce crystalline stoichiometric vanadium dioxide. [11] The quality of these deposited films is usually determined by optical and electrical conductivity measurements. [11, 34, 35]

Chosen Deposition Method

Samples for this study were deposited on a silicon wafer with a thermally grown amorphous silicon dioxide layer approximately 380 nm in thickness. A layer of amorphous vanadium oxide (VO_x), close in stoichiometry to vanadium dioxide, approximately 50 nm in thickness, was sputtered on top of the thermally grown oxide mentioned above. The sputtering took place by means of RF Magnetron Sputtering in a reactive environment with an oxygen partial pressure as part of the plasma. The deposited vanadium oxide wafer, as described, was obtained from Kevin Coffey at the University of Central Florida.[9]

1.3 Solid Phase Crystallization

Solid phase crystallization (SPC) has been extensively studied due to its application to the silicon industry [36–38]. The main goal of SPC is to give enough mobility to the atoms in an amorphous solid so that they may nucleate and allow those crystal nucleae to grow and form single crystals. This crystallization usually takes place by means of a "thermodynamic-driving-force," which may be accomplished by use of a furnace during an annealing process. [37]

The kinetics of the transition from amorphous material to crystalline material can be described by the "classical nucleation theory."[10] which is based on the capillarity effects at the crystal-amorphous interface. [37] The nucleation rate and the velocity of grain growth are explained by conventional thermodynamics. The energy required for nucleation carries two important factors: 1) The energy difference between amorphous

---

[9]For more details on the depositon parameters, refer to Appendix A

[10]For more details and references regarding this topic, the reader is encouraged to turn to "Thin Film Transistors: Materials and Processes" by Yue Kuo, 2004

and crystalline phases, ΔG_{ac} (proportional to volume); and 2) The energy required to maintain the amorphous-crystal interface (proportional to surface area). [37]

Figure 1.6 shows an energy diagram that helps explain the process of solid phase crystallization. In the energy diagram, the energies for the crystalline phase and the amorphous states are both local minima (labeled G_c and G_a respectively). Solid phase crystallization can take place as long as the crystalline state remains more "energy favorable" than the amorphous state. This means that free energy for the crystalline state is lower than the free energy for the amorphous state. The local minima between the crystalline state and the amorphous state are separated by an energy barrier. This energy barrier is due to the amorphous-crystal interface. In order to achieve solid phase crystallization, energy must be introduced into the system such that atoms found in the amorphous state (G_a) can overcome the barrier (G_1). The *rate* at which solid phase crystallization takes place depends, in part, on the size of the barrier (G_1), and how much more favorable the crystalline state is (ΔG_{ab}).[11]

As a summary, Solid Phase Crystallization through thermal methods involves giving enough thermal energy to the atoms in the film to overcome the energy barrier $(\Delta G_1$ in the figure) between the amorphous and crystalline states. In this manner, the atoms can find a more energetically preferred position in crystalline form. Annealing post-processing, (as mentioned in section 1.2) is a common technique for vanadium dioxide thin films.

---

[11]Other factors that affect the rate of solid phase crystallization also include: The probability of an atom to overcome the barrier, temperature, the atom's vibrational frequency, and the number of atoms at the amorphous-solid interface
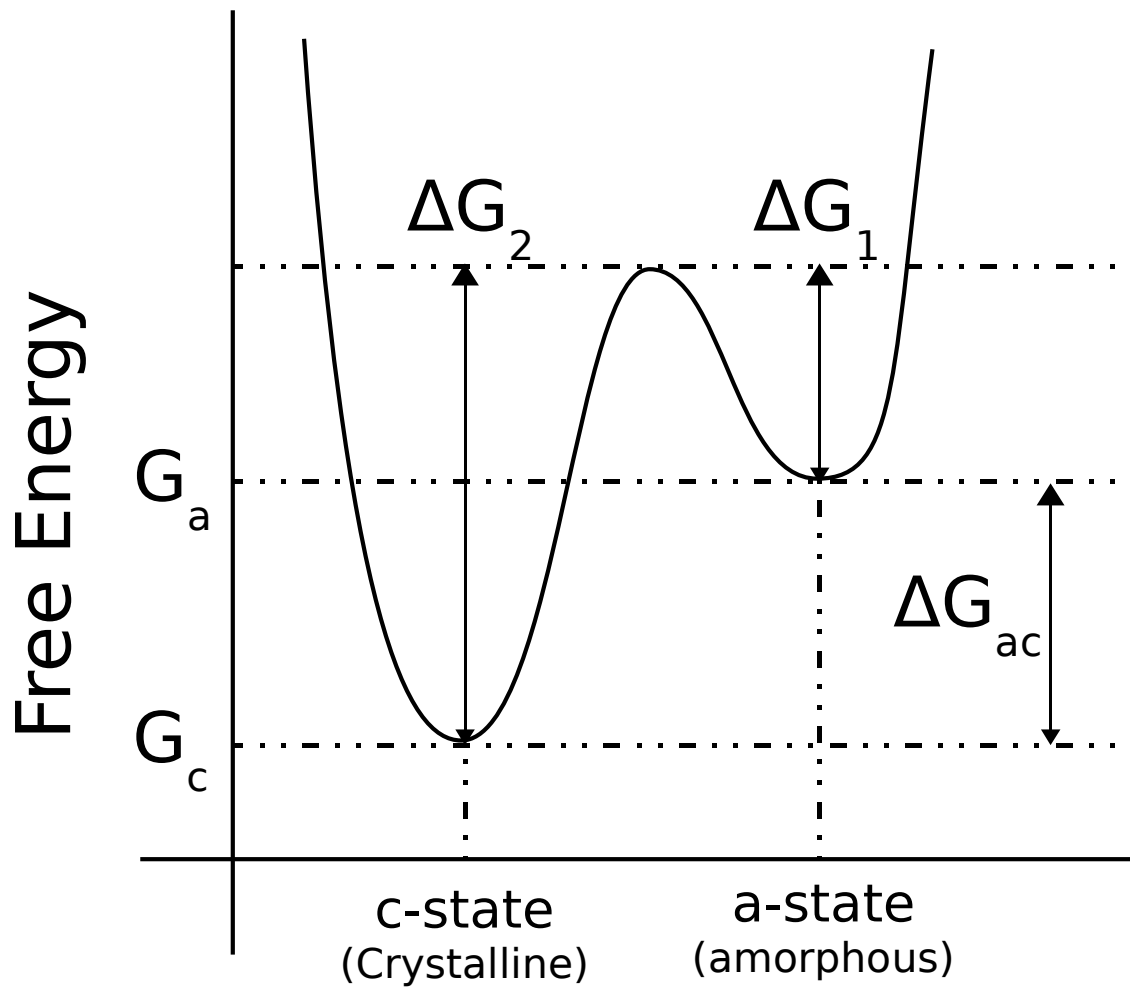
Figure 1.6 Schematic diagram of the free energy of amorphous and crystalline states. Kuo(2003). [37]

1.4   Methods for the Characterization of VO$_2$ Thin Films

As mentioned in section 1.2, there are various methods used to obtain vanadium dioxide deposited on a variety of substrates. Since the deposition of vanadium dioxide thin films is no trivial matter (see sections 1.1.1 and 1.2) it is imperative to determine the quality of the films produced. Naturally, these methods make use of the properties that set vanadium dioxide apart from other materials (see section 1.1.2). Though there are several methods employed to determine the quality of vanadium dioxide thin films, these can be categorized in three main groups: 1) Methods that rely on the crystal structure of vanadium dioxide; 2) Methods that rely on the oxidation state of vanadium; and 3) Methods that can observe the metal-to insulator phase transition that vanadium dioxide undergoes.

1.4.1   Characterization Based on the Crystal Structure of Vanadium Dioxide

As mentioned in section 1.1.2, the room-temperature state of crystalline vanadium dioxide is found in a monoclinic structure. This structure shears to become a tetragonal structure with lattice parameters $a = 4.54\mathring{A}$ and $c = 2.88\mathring{A}$. With the knowledge of the crystal structure, diffraction experiments may be conducted to help determine the quality of the resulting films. Diffraction methods constitute X-Ray Diffraction, Neutron Diffraction, and Electron Diffraction. (With their derivatives)

1.4.2   Characterization Based on the Valence States of Vanadium

The chemical composition of the films may also be examined through various characterization methods. The knowledge of the ratio of vanadium to oxygen atoms is another indicator of the quality of the deposited films. Spectroscopic techniques often yield information about chemical composition, and in some cases, they can also yield information about the valence states of some of the atoms. As mentioned in section 1.1.1, vanadium dioxide is only one of the many different vanadium oxides available. Thus knowledge of the oxidation state can help differentiate vanadium dioxide from other vanadium oxide stoichiometries.

Some of the techniques available that yield this kind of information include: X-ray Photoelectron Spectroscopy, Photo-Emission Spectroscopy, Raman Spectroscopy, Energy Dispersive X-Ray Spectroscopy, Electron Energy Loss Spectroscopy, and others. Usually during a spectroscopic study, a particular spectrum is collected and used as a "fingerprint" to determine the chemical composition, as well as the bonding states of the sample.

1.4.3   Characterization Based on the Electrical Change During the Metal to Insulator Transition

The other two types of characterization methods (previously) may be applied to a large variety of materials. However, this type of characterization seems to be somewhat particular to materials that undergo a metal-to-insulator transition. In the case of vanadium dioxide, the metal-to-insulator transition has been observed both optically and electronically.

Optical methods such as infrared laser spectroscopy, pulse-probe techniques, and

measurements in infrared transmission, absorbance, and reflection are used to observe the MIT and thus help determine the quality of the deposited vanadium dioxide.

Similarly, electrical measurements, such as resistivity, also help observe the MIT. In fact, the original report on vanadium dioxide's MIT was done through a resistivity measurement, and this method still is used today.

1.5 Scanning Electron Microscopy - a Tool for Characterization

The Scanning Electron Microscope (SEM) is a tool that allows for the imaging of small specimens with the use of an electron beam. The creation of the electron beam in the Scanning Electron Microscope is usually achieved in the following manner: 1) Electrons are extracted from a tip either thermally (thermionic emission) or by field emission; 2) These electrons are then accelerated towards an anode at a set potential difference from the tip; 3) The beam of electrons is then focused using magnetic lenses in order to make a fine probe.

In order to form an image, the electron beam passes through a set of scanning or deflector coils that shift the beam so that it may scan the sample (thus the name *Scanning Electron Microscope*). The beam is then allowed to interact with the sample and an image is formed by the interactions that take place between the electron-beam and the sample as the beam is scanned.

The interactions between the electrons and the sample allow for a rich amount of information that might be obtained in the Scanning Electron Microscope. Secondary Electrons, Backscattered Electrons, Characteristic X-rays, Auger Electrons, and Visible Light are among some of the "by-products" that take place during the scanning process. Depending on the detectors available, the SEM can be used to ob-

tain a wealth of information regarding the specimen. Typically, the image is formed by using a Secondary Electron Detector[12]. Nonetheless, there is more information that can be extracted from the Scanning Electron Microscope, and this information depends on the type of detector being used.

Under a typical imaging mode (secondary electron detector), the surface of the specimen is imaged without any other data collected. A useful aspect of the SEM under imaging mode is the ability to tilt the specimen. Imaging a surface where the electron beam is normal to the thin film is commonly called a "plan-view." Imaging where the sample is placed so that beam is parallel to the films is commonly referred to as a "cross-sectional view." Tilts in the specimen anywhere between a plan and a cross-sectional view will be referred in this work as tilted views. For a thin film, imaging the surface at different angles can give information regarding the morphology of the thin film, as well as give a rough estimate regarding the roughness of the surface.

The resolution available under a particular imaging mode is limited by the size of the probe achieved. The size of the probe depends on the "spot size" which determines the number of electrons used (current), the electron energy (determines the wavelength of the electron beam), and the focus of the beam (adjusted by the magnetic lenses). Contrast under this imaging mode depends on the angle between the electron beam and the features in the surface. In this manner, edges and corners are enhanced in the composed image. Figure 1.7 shows a rough schematic on how contrast is obtained in the Scanning Electron Microscope using the Secondary Electron Detector.

---

[12]The scanning electron micrographs obtained for this thesis were acquired using the Secondary Electron Detector.
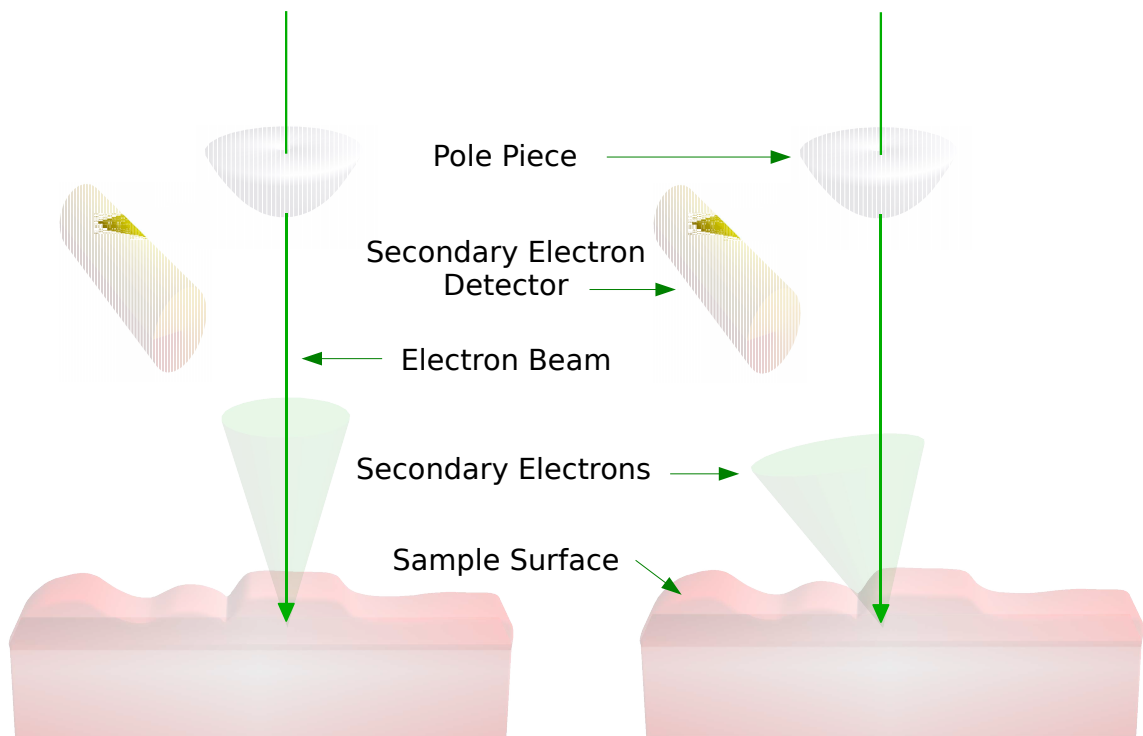
Figure 1.7　Using the Secondary Electron Detector in the Scanning Electron Microscope, contrast is obtained by the number of secondary electrons detected. The number of secondary electrons that "leave" the surface of the sample depends on the the angle between the main beam and the surface

1.5.1 Tilted View Surface Imaging

While plan-views allow for an initial view of the surface, a tilted view can give a rough estimate on the roughness of the film. Though it is not as quantitative as a roughness measurement in an Atomic Force Microscope, an estimated height profile for particles might be calculated. Further, a tilted sample is required in order to obtain Electron Back-Scattered Diffraction (EBSD) patterns, and to perform Orientation Imaging Microscopy (OIM) analysis.

1.5.2 Electron Back-Scattered Diffraction and Orientation Imaging Microscopy

As the electron beam interacts with the sample, the electrons in the beam scatter in all directions (but mainly in the direction of the beam). This will provide a virtually endless supply of electrons traveling in all directions (see figure 1.8). If the sample is crystalline, then several of the scattered electrons inside the sample will find themselves in the Bragg condition. These electrons will scatter multiple times while remaining in the Bragg condition. This creates a "channeling" effect that allows electrons to escape the sample creating observable contrast. (See figure 1.9) These multiple scattering events (along with the radial symmetry rising from having electrons scattered in all directions) creates Kossel Cones. Since most of the electrons that enter the sample scatter in the forward direction (figure 1.8) a tilted sample provides the benefit of having a larger number of the scattered electrons close to the surface and able to exit the sample. [39–42]

The intersection of the Kossel Cone with the Ewald Sphere creates the condition necessary to observe a set of Kikuchi lines. Figure 1.10 shows a diagram of the Kossel cones, the (hkl) plane they represent, and the observed Kikuchi lines. Since the
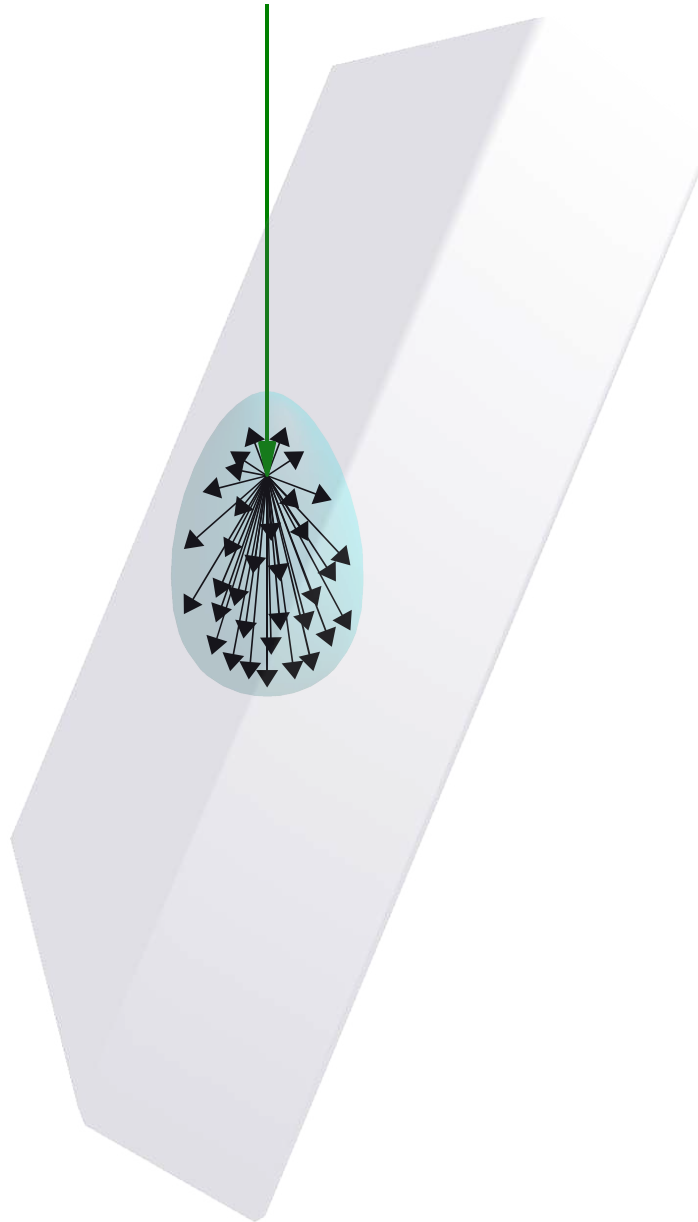
Figure 1.8 As the electron beam interacts with the sample, electrons will scatter in all directions (but with a preferential scattering direction following the direction of the beam).

Kossel Cone

Scattered
Electrons in the
Bragg Condition

θ_{Bragg}

(*hkl*) planes
in the specimen
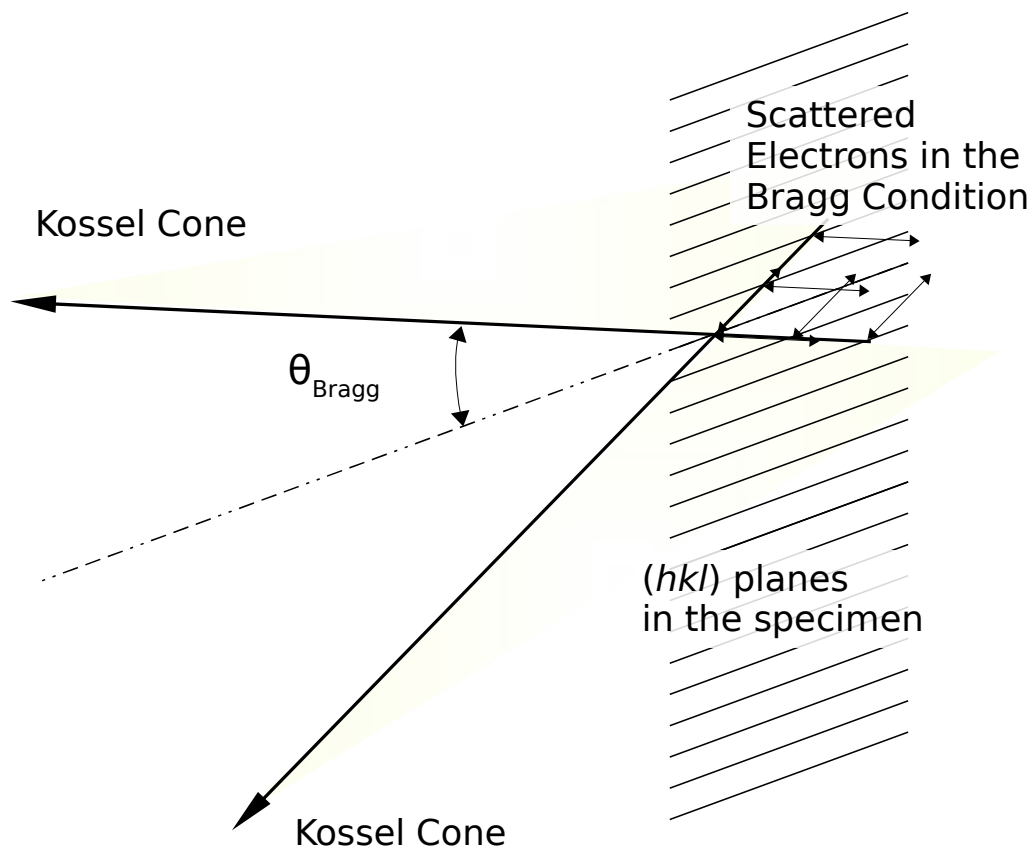
Kossel Cone

Figure 1.9 Since the electrons from the main beam scatter in all directions, a number of them will find themselves in the Bragg condition. Kossel cones are created from all the electrons scattering in the Bragg condition.
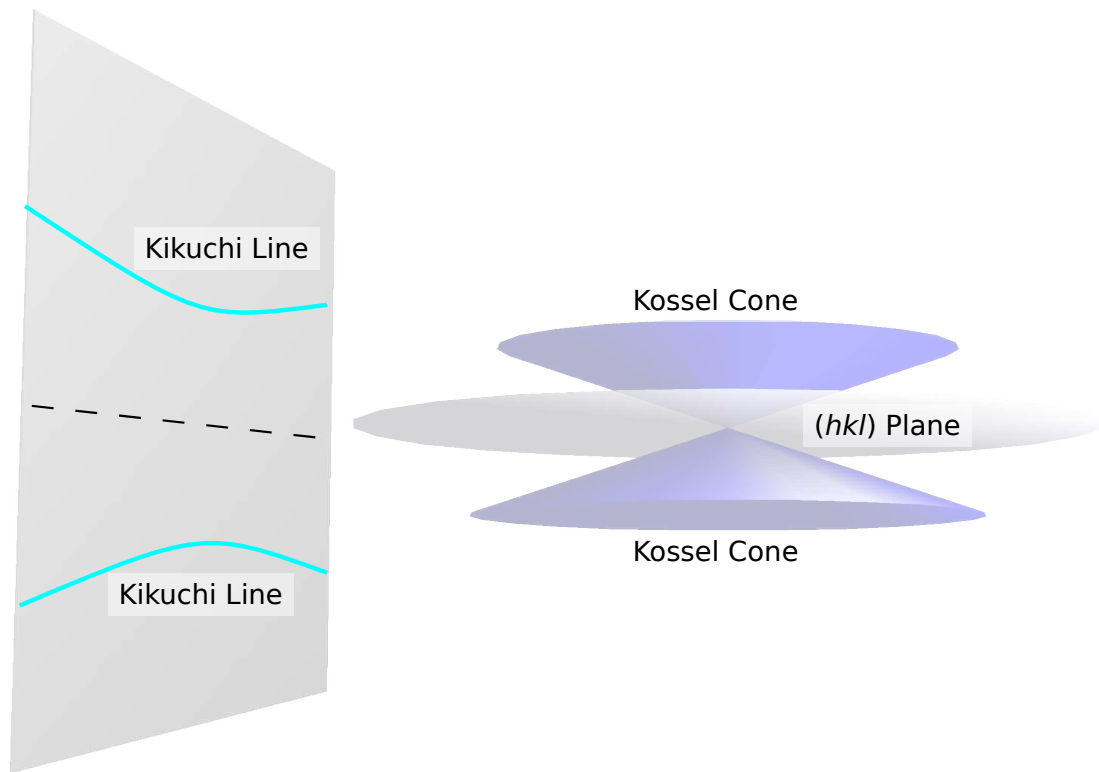
Figure 1.10 Kikuchi lines are the intersections of Kossel cones with the phosphor screen. (The bands are actually hyperbolic not parallel. However, due to the small angle between the plane and the cone, they look like parallel lines in practice.)

Kikuchi lines are formed by the intersection of a plane with a cone, they are conic sections (in this case, hyperbolas). However, since the angle between the plane and the Kossel cone is small, these kikuchi bands will look like lines.

A full Electron Back-Scattered Diffraction (EBSD) pattern is formed by all the kikuchi lines that intersect the phosphor screen (See fig. 1.11). A full Orientation Imaging Micrograph can then be performed. This is done by letting the software be in charge of collecting EBSD patterns while a scan of the surface takes place. The software then indexes each of the patterns collected, keeping them referenced to the position where they belong. By this method, a map of the surface may be

Pole piece

High current e-beam

Back-Scattered Electrons

Electron Back-
Scattered Diffraction
Pattern

Phosphor Screen
and CCD

Tilted Sample
Θ~70°.
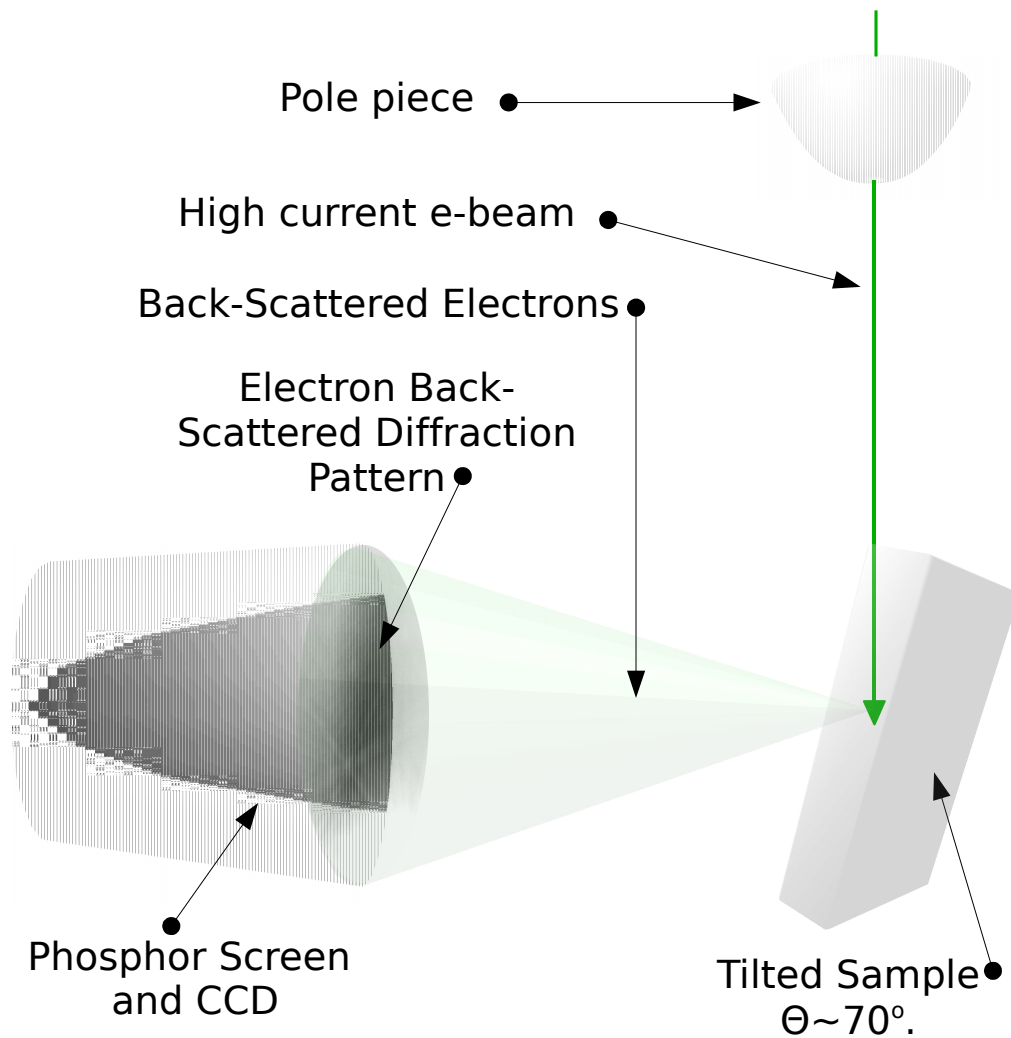
Figure 1.11   As the electron beam interacts with the sample, some of the electrons will be "back-scattered" in the Bragg Condition. These electrons will form Kikuchi patterns that can be detected with a phosphor screen and a camera. In Orientation Imaging Microscopy, Kikuchi patterns are recorded and indexed as a scan takes place in the Scanning Electron Microscope.

created where individual grains are selected by sections of the scan having the same orientation. This method helps determine orientation of the grains in the surface, misorientations between grains, and grain sizes (see figure 1.12). The attainable resolution depends on factors such as the beam size, scan parameters, and quality of the sample. Figure 1.13 shows a typical OIM scan, where the particle size can be used to determine how fine of a scan to perform for OIM.

1.5.3   Simulated Electron Back-Scattered Diffraction Patterns

Electron Back-Scattered Diffraction (EBSD) patterns may be simulated as they depend on the structure of the material observed. Since EBSD is a diffraction technique, [41] it can be used to index different crystallographic structures. Further, since the crystal structures among the different vanadium oxides varies considerably[13], EBSD is a good candidate for characterizing resulting vanadium dioxide thin films. Crystal structures, as the ones mentioned in sections 1.1.1 and 1.1.2 may be used to generate possible EBSD patterns. Figure 1.14 shows some calculated diffraction patterns for several vanadium oxide stoichiometries, including two phases for vanadium dioxide, along with the orientation that would yield such patterns. The software available for OIM uses these calculated diffraction patterns to compare them against obtained EBSD patterns. Some of the characteristics that are used for indexing the patterns obtained include the angle between bands, distance among zones, and number of zones seen in the pattern. As observed from the calculations in figure 1.14, the change in symmetry of VO_2 yields some missing bands, but otherwise, the VO_2 patterns are rather similar.

---

[13]see sections 1.1.1 and 1.1.2
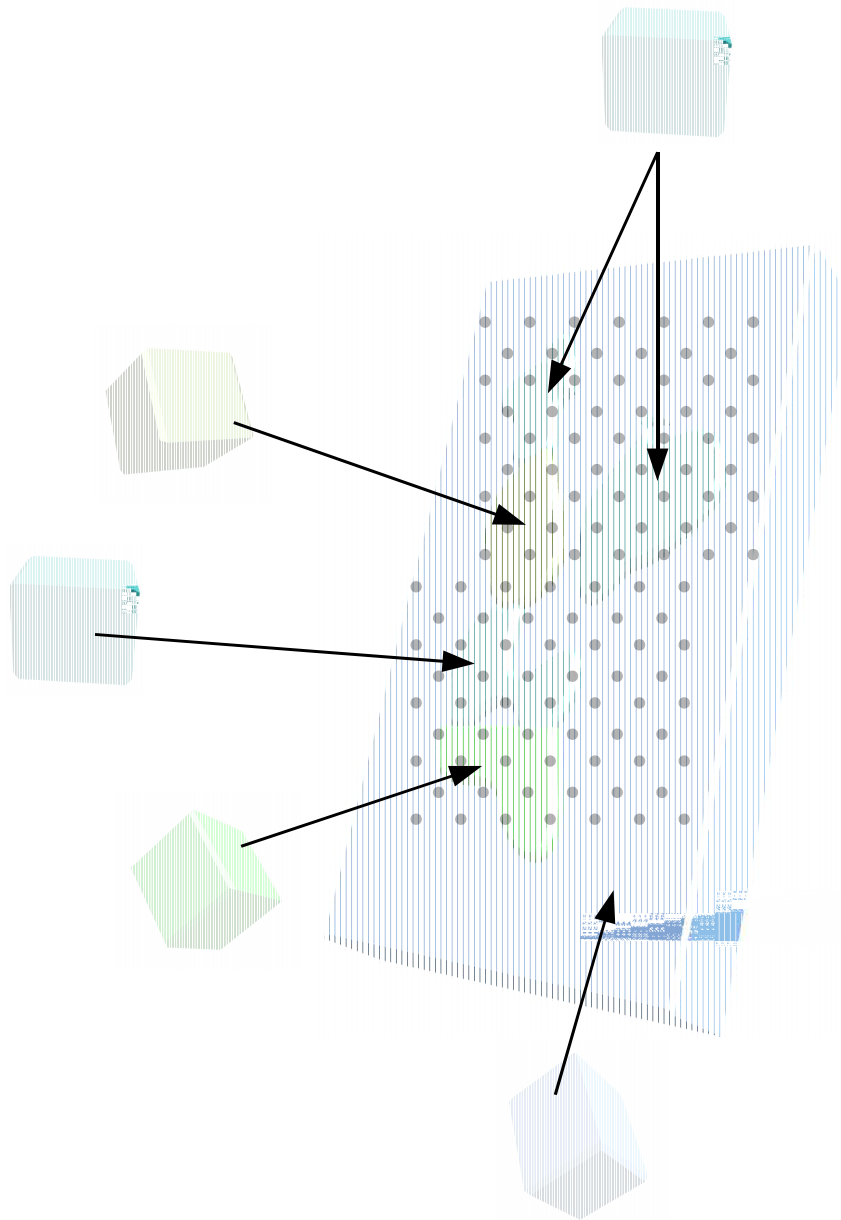
Figure 1.12 In an Orientation Image Micrograph the features, such as grain shapes and sizes, are determined by the crystal orientation. Resolution of this technique is determined by the beam size, scan parameters, and quality of the sample.
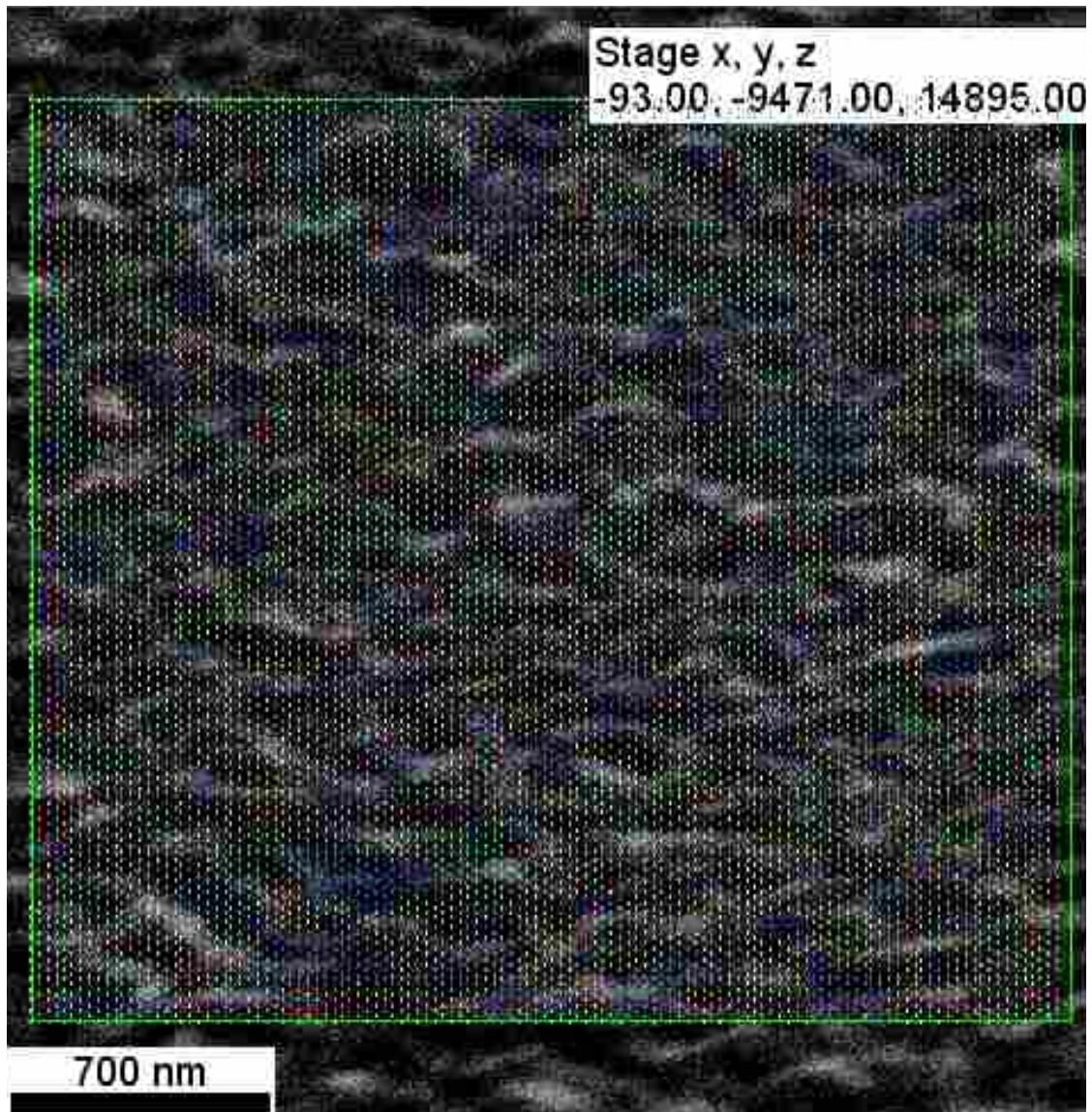
Figure 1.13 (color) During an OIM scan two important factors to consider are the grain size, and the scan size. In this sample image, the grain size is approximately 300 nm across and the distance between sampling points is about 50nm.
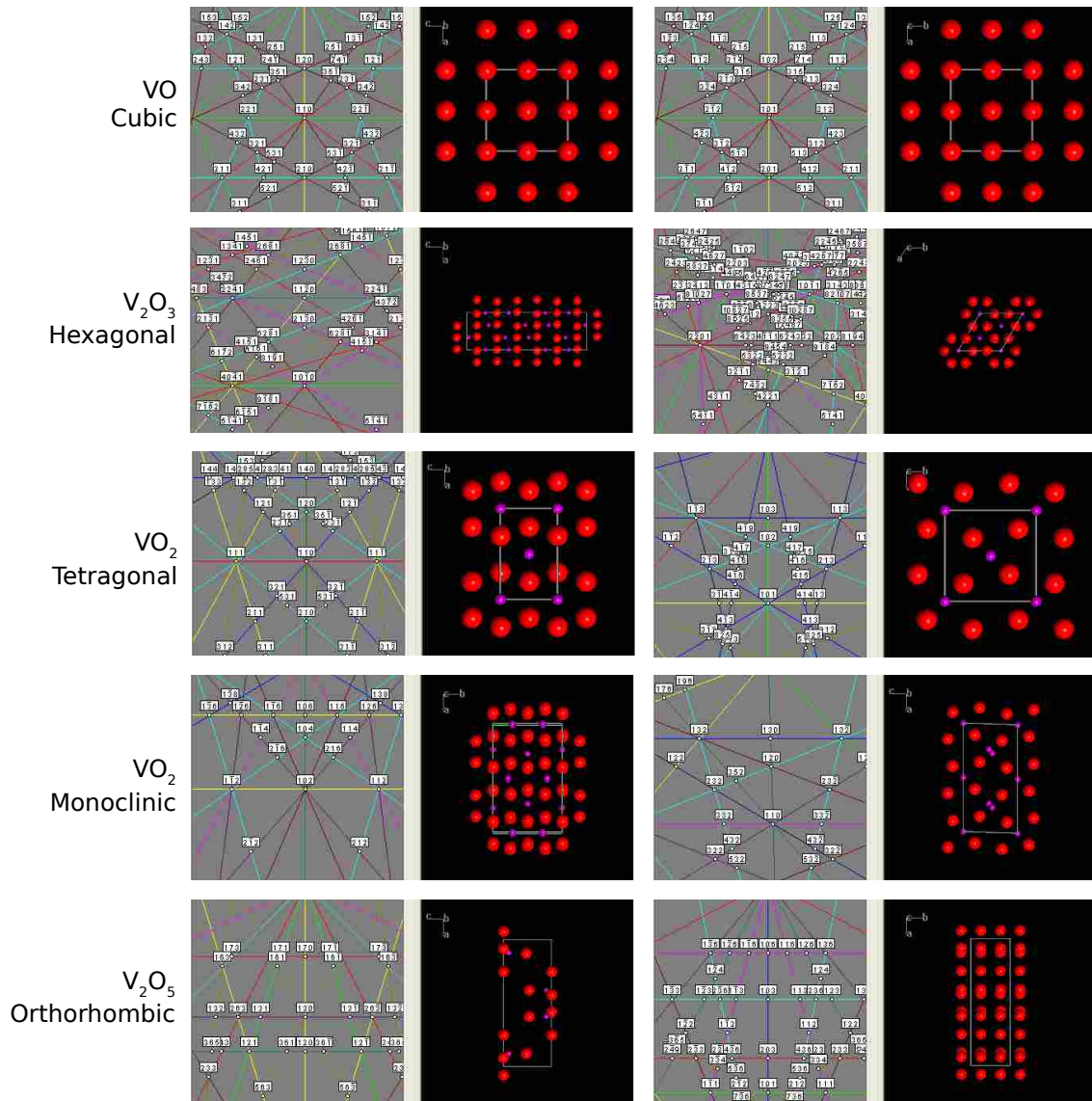
Figure 1.14 Calculated EBSD patterns for VO, V_2O_3, VO_2 tetragonal, VO_2 monoclinic, and $V_2 O_5$. The patterns calculated from the VO, V_2O_3, VO_2, and $V_2 O_5$ are distinctive enough to distinguish between them.

1.6   Purpose for this Thesis

The purpose of this project is to carry out the solid phase crystallization of amorphous vanadium dioxide thin films and their characterization with the scanning electron microscope. The synthesis of vanadium dioxide is not trivial, as variations in the vanadium to oxide ratio will display different electronic properties. Further, as mentioned in section 1.1.2, there is evidence to show that the characteristics of the metal to insulator transition in VO_2 varies depending on grain size. Thus, characterization of the resulting films, down to their microstructure, is of crucial importance.

Each of the samples will undergo characterization through Scanning Electron Microscopy (SEM), in conjunction with Orientation Imaging Microscopy (OIM), to determine the topography, crystallinity, and quality of the samples produced. The characterization process will then allow for further study on the properties of vanadium dioxide micro and nanocrystals.

Chapter 2

VO$_2$ Solid Phase Crystallization of Vanadium Dioxide Thin Films and Characterization Through Scanning Electron Microscopy and Orientation Imaging Microscopy

2.1   Methods

A 200 mm wafer used for this study was provided by Kevin Coffey[1] at the University of Central Florida. The characteristics of this wafer are described in section 1.2. Pieces of this wafer were cleaved to squares approximately 5 mm on the side. These individual squares were then subject to the following process:

1. Samples were annealed with temperatures ranging from 200°C up to 1000°C

---

[1]To whom the author would like to express his sincerest gratitude.

and times ranging from 17 hrs down to 5 min.

2. Samples were imaged in the Scanning Electron Microscope to observe any noticeable changes.

3. Electron Back-Scattered Diffraction patterns were attempted to test for crystallinity.

4. If crystalline, an orientation scan was performed and analyzed.

2.1.1 Solid Phase Crystallization - Annealing Procedure

Annealing conditions ranged from 200°C for more than 15 hrs up to 1000°C for 5 min. Depending on the environment or the time, annealing process varied slightly. The two environments chosen to anneal in were air and argon. In both cases, the temperature quoted was that reported by the temperature controller, and it was noticed to "ring" within 2°C upon reaching the set temperature.

Air Environment

For the anneals performed in air the furnace in figure 2.2 was used. The sample was placed inside the furnace, allowing it to be as close to the center of the tube as possible. The temperature controller was then programmed to ramp up to the selected temperature at the rate set by the controller. The temperature was held there for a specified amount of time and then allowed to cool down. Figure 2.1a shows a diagram of a typical annealing program.

Argon Environment

The furnace for this annealing process was manufactured by "Lindberg-Blue." (See Figure 2.3) The furnace uses a quartz tube to hold the sample in, while being able
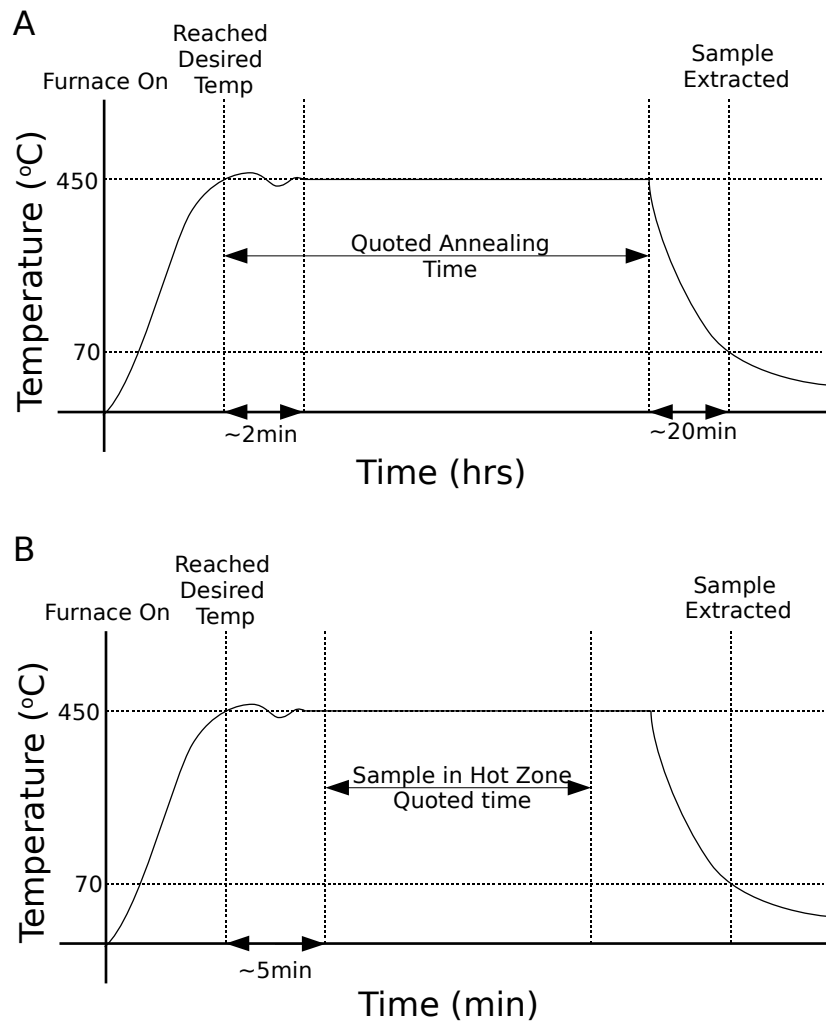
Figure 2.1 Temperature vs. time diagram depicting a typical annealing cycle. The temperature controller was allowed to ramp up at its default rate to the set temperature. There was a slight "ringing" once the set temperature was reached of (at most) 2°C. The annealing time ranged from about 5 min to 17 hrs before the furnace was allowed to cool down. Long term anneals (> 1 hr) followed program A, where the sample was placed in the hotzone for the whole process. Short term anneals (< 1 hr) followed process B where the sample was inside the furnace, but away from the "hot-zone" and was brought into the "hot-zone" only for the specified annealing time.

Figure 2.2 Furnace used for the anneals done in air.

to control the environment in which the annealing takes place. Individual pieces are placed inside of the tube as close to the center of the tube (radially) and as close to the the thermocouple as possible (length-wise) (see figure 2.4). Samples were initially placed inside the quartz tube as close to the thermocouple as possible, with a few exceptions described below. The argon environment was controlled by flowing argon gas through the quartz tube. The argon used was 99.9% purity. Rubber seals were used in the inlet and outlet of the tube to prevent air from the surroundings to enter into the tube (see figure 2.5). A positive pressure was kept iniside the quartz tube by using a vacuum oil bubbler gas outlet and a constant flow of argon into the tube. The flow rate used for these anneals was a constant 600 sccm as controlled by a Mass Flow Controller (see figure 2.6).

For the cases where the anneals were on the order of one hour or longer, the sample was placed inside the furnace and the conditions mentioned above were set before any annealing took place inside the furnace. Upon ensuring that the setup was correct, the furnace was allowed to purge (at room temperature) for 10 minutes in order to eliminate the air inside the quartz tube. The furnace's temperature controller was then programmed to ramp up to the selected temperature at the rate set by the controller. The temperature was held there for a specified amount of time and then allowed to cool down (see figure 2.1A). This whole process was completed maintaining the argon flow until the sample cooled down to below 100°C. At that point, the annealing chamber was opened and the sample extracted.

For the cases where the anneals were 30 min or less, the process in figure 2.1b was followed. In this process, the sample was initially placed inside the furnace, however it was placed away from the "hot-zone." The outlet in the argon furnace was outfitted with a "T" joint to allow for a guiding rod to move the sample into and out of the "hot-zone" (See figure 2.5). This technique allowed the placement of

Figure 2.3 Furnace used to perform the argon anneals in.

Figure 2.4 Furnace used to perform the argon anneals. The ability to open the furnace allows for easy placement of the sample close to the thermocouple (located in the middle).

Figure 2.5 Both inlet and outlet to the quartz tube are fitted with a rubber "O"-ring to form an air-tight seal. Further, the outlet was outfitted with a "T" joint to allow a guiding rod to move the sample into and out of the "hot-zone." (Here, the "T" joint is plugged as it is not being used)

Figure 2.6 Mass Flow Controller used to control the argon flow.

the sample to within 2 mm of the zone. The conditions mentioned above were set before any annealing took place just like mentioned previously. Upon ensuring that the setup was correct, the furnace was again allowed to purge (at room temperature) for 10 minutes in order to eliminate the air inside the quartz tube. The furnace's temperature controller was then programmed to ramp up to the selected temperature at the rate set by the controller. At this point the sample was moved into the "hot-zone," the sample kept there the specified amount of time, and then moved out of the "hot-zone." The furnace was then allowed to cool down. This whole process was completed while maintaining the argon flow until the furnace cooled down to below 100°C. At that point, the furnace was opened and the sample extracted.

2.1.2 Surface Imaging Through Scanning Electron Microscopy

The Physics and Astronomy Department at Brigham Young University is equipped with a Phillips XL30 Scanning Electron Microscope (figure 2.7). This particular microscope is equipped with several detectors, including a detector for Orientation Imaging Microscopy. Further, this instrument has an "Ultra High Resolution" (UHR) mode that gives the ability to obtain spatial resolution in the nanometer range.

Figure 2.7 Phillips XL30 Scanning Electron Microscope. Shown in the picture are also the SE, the XEDS, and the EBSD detectors

After the annealing process took place, the samples were mounted onto an aluminum SEM stub. Adhesion to the stub was accomplished by means of colloidal graphite in order to ensure a conductive path from the sample onto the SEM stub (see figure 2.8). The colloidal graphite was diluted using isopropanol (allows for quicker drying) It was of great importance to ensure the complete drying of the colloidal graphite to prevent contamination from hydrocarbons inside the SEM vacuum.
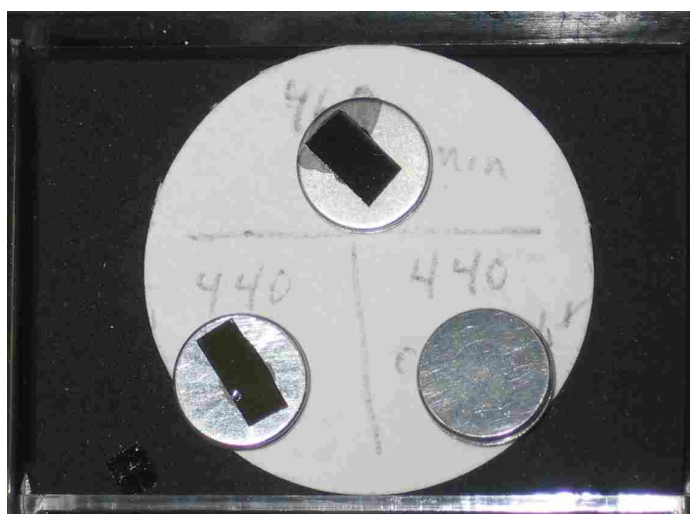
Figure 2.8 Samples were mounted onto a SEM stub by means of colloidal graphite in order to ensure a conductive path from the sample onto the stub.

Both "plan-views" and "tilted-views" were acquired through the SEM. The conditions under which the images were acquired depended upon the type of image desired.[2] The specific conditions of the beam, such as spot size, accelerating voltage,as well as the detector used, were recorded with each image taken. It was imperative to be able to find a distinguishable feature (any feature) in order to be able to properly focus the image and correct for astigmatism. As the image is magnified, the focus

---

[2]The accelerating voltage can be as low as 1 kV and as high as 30 kV. Spot sizes are labeled from 1 to 7 where a smaller number indicates a finer probe. Usual imaging under this mode is best achieved with a spot size of 3, a 5 kV accelerating voltage, and placing the sample at a working distace of 5 mm. UHR mode can also be used under these settings.

and stigmators are manually corrected. The image was usually magnified as high as the spot size and voltage permit, while ensuring that the focus and astigmatism were corrected. Most images were then taken at a lower magnification, while the probe remained as fine as possible and better detail might be extracted from the image.

Plan-View Surface Imaging

In order to obtain a plan-view image, the sample sits perpendicular to the beam. Figure 2.9 shows the inside of the SEM as the sample sits ready to be imaged in plan-view. This condition allowed for a "top-down" view of the sample. Grain sizes were observed and their length and width measured. Unfortunately, height information and roughness are not accessible with this view.
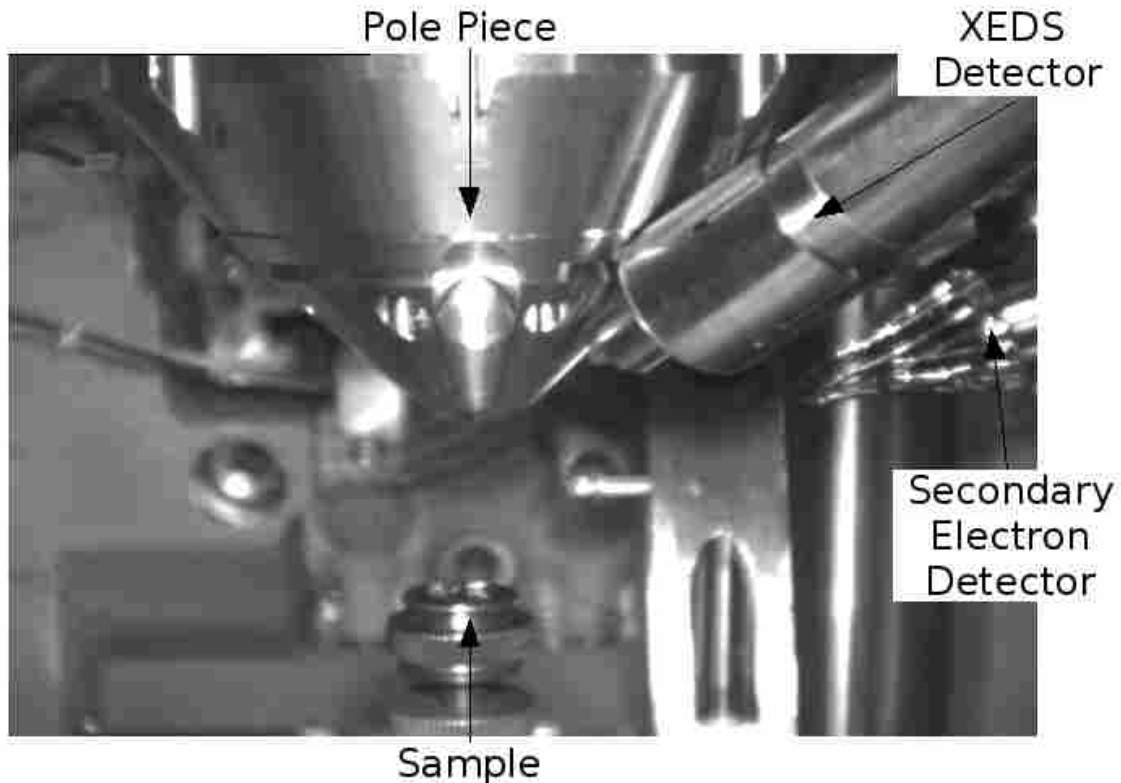
Figure 2.9 Interior of the Phillips XL30 SEM set for a plan-view image. The sample sits perpendicular to the beam.

Tilted-View Surface Imaging

The XL30-SEM allows for the sample to be tilted. The tilt allows for an estimate of the height and roughness of a surface. Although the height information cannot be quantified as well as an atomic force microscope (AFM) would, qualitative roughness may be seen. In order to tilt the stage, the sample was moved further away from the pole piece as a safety precaution.[3] In order to carry out Orientation Imaging Microscopy (OIM) the sample was tilted at 70°. Figure 2.10 shows the inside of the XL30-SEM with the sample tilted ready to acquire an EBSD pattern.

Figure 2.10 Interior of the Phillips XL30 SEM set for a tilted-view. The normal to the sample is 70° away from the beam. These conditions are necessary to perform an OIM scan. The EBSD detector has been inserted into the SEM.

---

[3]Due to the tilting, the sample itself moves, so if it is desired to image the same area with a plan-view and a tilted-view, the working distance of the sample should be taken into account.

2.1.3 Electron Back-Scattered Diffration Characterization and Orientation Imaging Microscopy

With the sample tilted so that the normal of the plane is 70° away from the electron beam, EBSD patterns were obtained. The working distance of the sample was such that the back-scattered electrons hit the phosphor screen (see figure 1.11). The sample's x, y, and z, coordinates were taken with respect to the stage itself, not with the beam. Thus, in order to change the working distance (distance to the pole piece) the y and z coordinates of the sample were manually adjusted.[4] The EBSD detector and the SE detector were used simultaneously in some instances. In this manner, the working distance was adjusted so that the highest signal was detected in the EBSD detector, while keeping the area of interest imaged. Typically, a working distance of 12 mm was optimal. (see figure 2.10)

In order to achieve an indexable pattern, enough electrons must hit the phosphor screen so that an image is formed. This requirement in current limited the available beam conditions and it was usually achieved with an accelerating voltage of 25 kV and a spot size of 6. With this beam condition, the spatial resolution in the SEM was greatly diminished.[5]

The technique of OIM is based on collecting EBSD patterns from different areas in the sample and forming an image based on the orientation of the grains (see section 1.5.2.

---

[4]The SEM software does not seem to provide an automated process that can achieve this

[5]Finer scans may be attempted with smaller spot sizes, but at the expense of longer collection time, danger of sample drift, and possible contamination to the sample.

Electron Back-Scattered Diffraction on VO$_x$

Crystallinity of the annealed VO$_2$ samples was tested by EBSD. The SEM was set as described previously and shown in figure 2.10. Even though the EBSD detector and the SE detector can be used simultaneously as described before, individual patterns are collected from spots in the surface. Thus, the imaging of the surface is "frozen" so that the beam can be placed in a specific spot and the pattern collected.

If, and only if, the beam is placed in a large enough crystal, a EBSD pattern will be formed. If not, no line patterns will be observed. Since there is the possibility of crystals in different orientations, individual patterns may be difficult to observe. Some steps were taken in order to enhance the EBSD patterns collected:[6]

1. A background image was obtained while a SEM image is being obtained. This way, the background image was an average of the patterns in all the area within the SEM view.

2. When a EBSD pattern was collected from a specific spot, the background image was subtracted in order to help enhance the image.

By doing these steps, crystallinity of the sample may be observed. The software was used to index the pattern obtained and compared with a list of pre-loaded calculated EBSD patterns for indexing (see section 1.5.3). Identification of the crystals observed was carried out at this time. It is also during this stage where the average exposure time was determined in order to obtain indexable patterns.

Indexing of the acquired EBSD patterns was based in several criteria:

1. Observed crystallographic zones

---

[6]The software offers several tools to digitally enhance the EBSD patterns collected. It was found that a simple background subtraction was more than adequate.

2. Observed Kikuchi bands

3. Angles between Kikuchi bands

4. Kikuchi band widths

These parameters were compared with the calculated EBSD patterns. Using these parameters, each obtained EBSD pattern received a number of "votes" as well as a confidence index as to what material offers the best match.

Orientation Imaging Microscopy

As mentioned in section 2.1 it is only after crystallinity is confirmed that an OIM scan was set.[7] Using the SE detector, a micrograph was obtained and used as a reference. Based on the obtained micrograph, an area was selected in which to perform the scan. Also, based on the micrograph, the separation between probing points was determined and a grid selected. As a goal, a grain was probed about 40 times[8] using a hexagonal grid. EBSD patterns were then collected using the array set. Figure 2.11 shows a typical setting for an OIM scan. Notice that due to the high tilt, the software was only able to sample each grain about 40 times (4 rows of 10 samples each).

The software automatically moved the probe, waited for the EBSD pattern to be collected, indexed the pattern, and saved the location of the probe and the pattern's index and orientation.[9] Analysis of the data then permitted the creation of Orientation Imaging Micrographs (OIM maps) and extraction of other data.

---

[7]No attempts were made to perform OIM scans on films where no indexable patterns were seen.

[8]Due to the high tilt, usually a grain was probed in a grid where 10 images were taken horizontally and 4 vertically.

[9]In practice, only the index and orientation information is saved. The actual pattern is *NOT* saved.
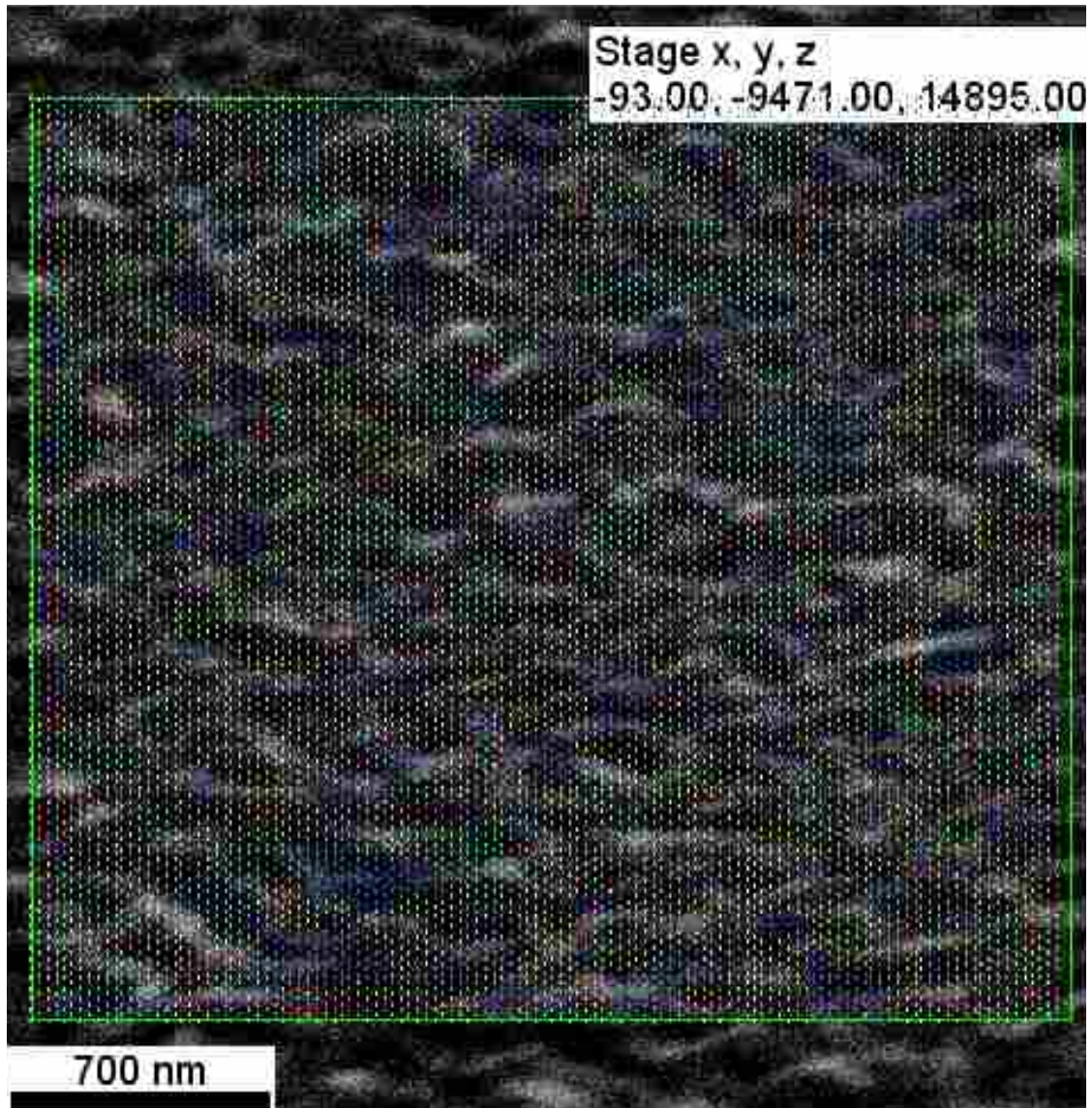
Figure 2.11 [Color] In the Background, an SEM image is used as a reference. Recall that the sample is tilted 70°. An area is selected to perform an OIM scan, the separation between samples is specified, and the type of grid chosen. In this case, an area approximately 3μm (along the x direction) is probed every 50 nm using a hexagonal grid.

Naturally, the orientations obtained from the OIM scans depended on the position of the sample. Figure 2.12 shows the convention used. The Normal Direction (ND) is the direction normal to the surface. The Reference Direction (RD) is the direction set by the Electron Beam. It can be easily thought of as the direction that is: 1) parallel to the plane made by the Electron Beam and its reflection off the surface, and 2) on the sample's surface. Finally, the Transverse Direction (TD) is the direction perpendicular to ND and RD that lies on the surface of the sample.
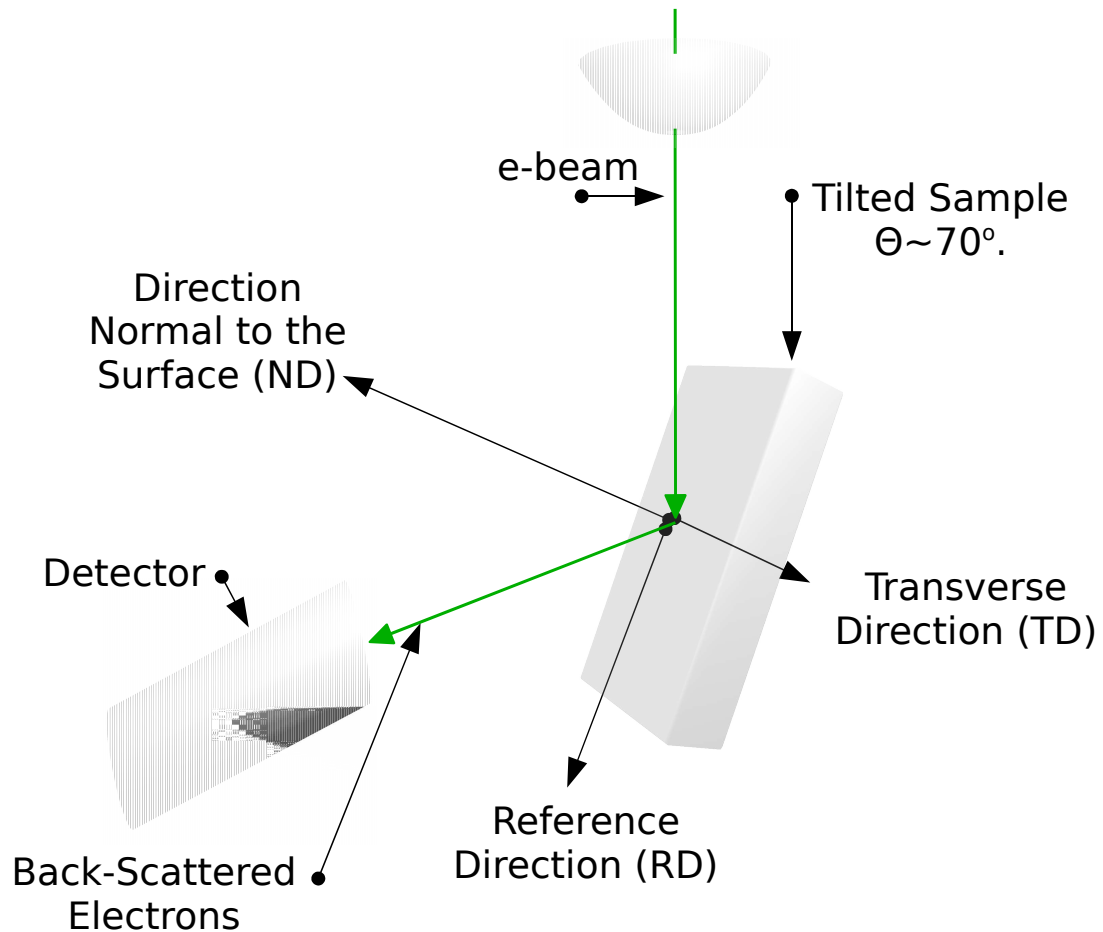
Figure 2.12 Conventions used to determine orientation on a sample: Normal Direction (ND), Reference Direction (RD), and Transverse Direction (TD).

2.2 Results of the Annealing in an Argon Atmosphere

As described in section 2.1: The films were subjected to an annealing process in order to achieve Solid Phase Crystallization; then characterized through Electron Back-Scattered Diffraction; finally an Orientation Imaging Micrograph is obtained. The results for the anneals performed in an argon atmosphere are presented in the following subsections.

2.2.1 Morphology of the Solid Phase Crystallization Observed in the SEM

Table 2.1 summarizes the annealing conditions for individual samples, as well as the average grain sizes obtained. Changes in the surface are evident from the micrographs shown in Figure 2.13. Higher mobility was observed for higher temperatures. At 1000°C, grain growth was limited by the amount of material available. This was evident from the formation of grain sizes up to 1 μm in length. Isolated particles decreased in size as temperature decreased. It was observed that 500°C showed the formation of individual grains when given a large time to grow and semi-continuous films for shorter times.

Continuous and semicontinuous thin films were obtained with anneals between 400°C and 450°C. Again, temperature and time helped determine the size of the grain obtained.

Under argon anneals, no change in the surface was observed for anneals under 300°C.

Temperature °C	˜10 min	˜30 min	˜1 hr	˜10 hrs
< 300	–	–	–	NCO
400	–	–	NCO	50 nm*
440	NCO	NCO	IC	100 nm
450	NCO	IC	200 nm	250 nm
500	300 nm	500 nm (IP)	–	–
680	500 nm(IP)	500 nm(IP)	–	–
1000	LIP> $1\mu m$	LIP> $1\mu m$	–	–

Table 2.1 Average particle size resulting from annealing process in argon. The following labels are used: NCO - "No Crystallization Observed"; IC - "Inconclusive"; IP - "Isolated Particles"; LIP - "Large Isolated Particles"; finally, a "dash" $(-)$ is placed for those conditions not tested. *The 400 nm film yielded EBSD patterns, but the quality of the patterns obtained was quite faint and not easily indexable.

Annealed at 1000ºC for 7min

Annealed at 500ºC for 1hr (70º tilt)

Annealed at 400ºC for 17hrs

Amorphous

Annealed at 450ºC for 17hrs
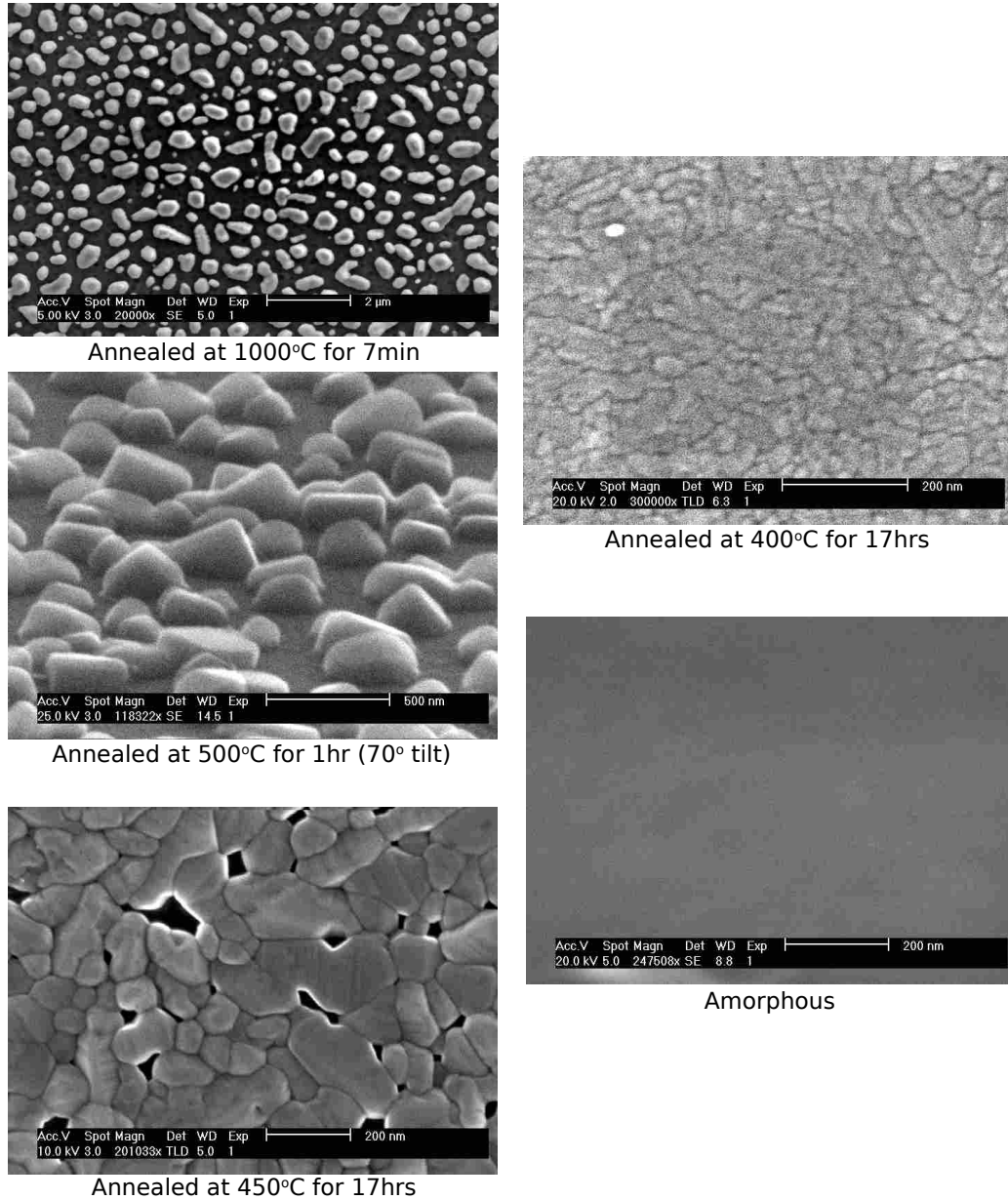
Figure 2.13 Scanning electron micrographs of the resulting films annealed under various conditions. Scale bars vary from 2 μm in the 1000°C anneal down to 200 nm in the 450°C anneal. Grain growth is evident as a function of temperature. Higher temperatures showed higher mobility as larger and isolated grains are formed.

2.2.2 Characterization Through Electron Back-Scattered Diffraction

Figures 2.14 and 2.15 show an EBSD pattern obtained from a sample annealed at 450°C for 17 hrs. This pattern is characteristic of patterns obtained from the anneals performed at 440°C above. The indexing shown in figure 2.14 indicates a match for vanadium dioxide. The zones, lines, and band widths are a good match for the structure files provided. From the patterns obtained the vanadium dioxide files received the highest number of votes. There was no evidence of any other vanadium oxides present.

However, it was also observed that the EBSD patterns obtained matched the calculated EBSD patterns for the three VO_2 structure files used. As shown in figure 2.15, the calculated EBSD patterns are not different enough for the software to distinguish between them. The pattern that received most of the votes and a high confidence index was usually the tetragonal structure file. It was also noticed that the pattern used for the monoclinic (stressed) phase of VO_2 (though it received high votes) was marked with a zero confidence index due to its pseudo-symmetry. Due to the many similarities in the structures of VO_2, the tetragonal file was used for the OIM scans as it was easier for the software to index.[10] (See figure 2.15)

The clarity of the patterns obtained played a big role in the ability of the software to reliably index the films. For the sample annealed at 400°C the quality of the EBSD patterns was so low that the software could not index the patterns automatically (thus an OIM scan was not performed). However, several patterns were obtained in different areas of the film and manually indexed as VO_2 using the tetragonal EBSD pattern.

---

[10]Recall, the grain formation and orientation took place during the annealing process, when VO_2 is at a high temperature and, thus, in the tetragonal phase. So it makes sense to use this crystal structure for indexing.

This was seen as a limit in this technique as OIM could not be performed on this sample.
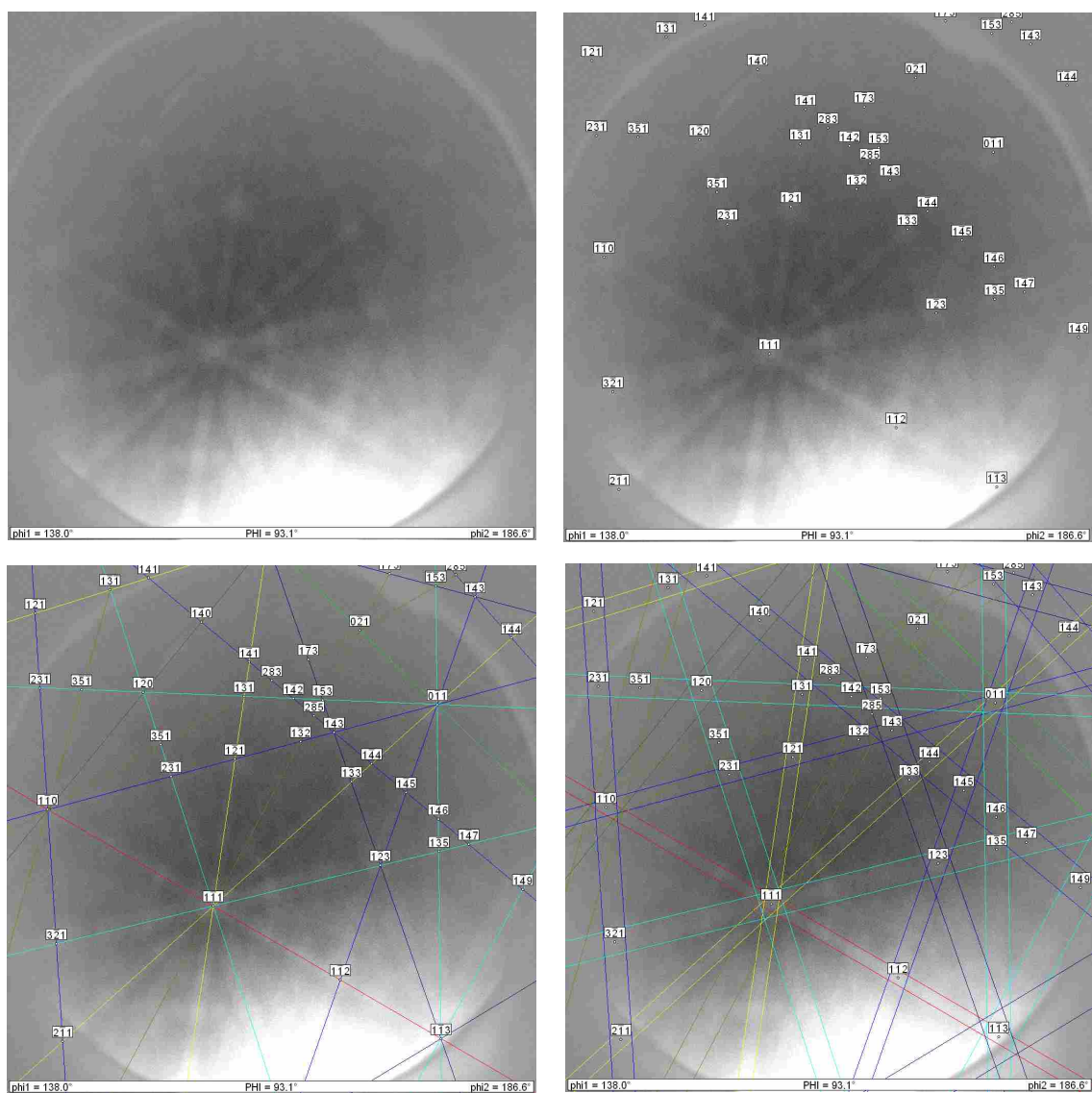
Figure 2.14 Electron Back-Scattered Diffraction Pattern obtained from the sample annealed at 450°C for 17 hrs. Indexing of the pattern can take place by labeling the acquired zones, or observed bands, and even by the band widths. This pattern is characteristic to the patterns obtained from the produced films under an argon anneal, indicating crystalline vanadium dioxide.

EBSD pattern as obtained

EBSD pattern – Tetragonal index

EBSD pattern – Monoclinic index

EBSD pattern – Monoclinic (Stressed) index
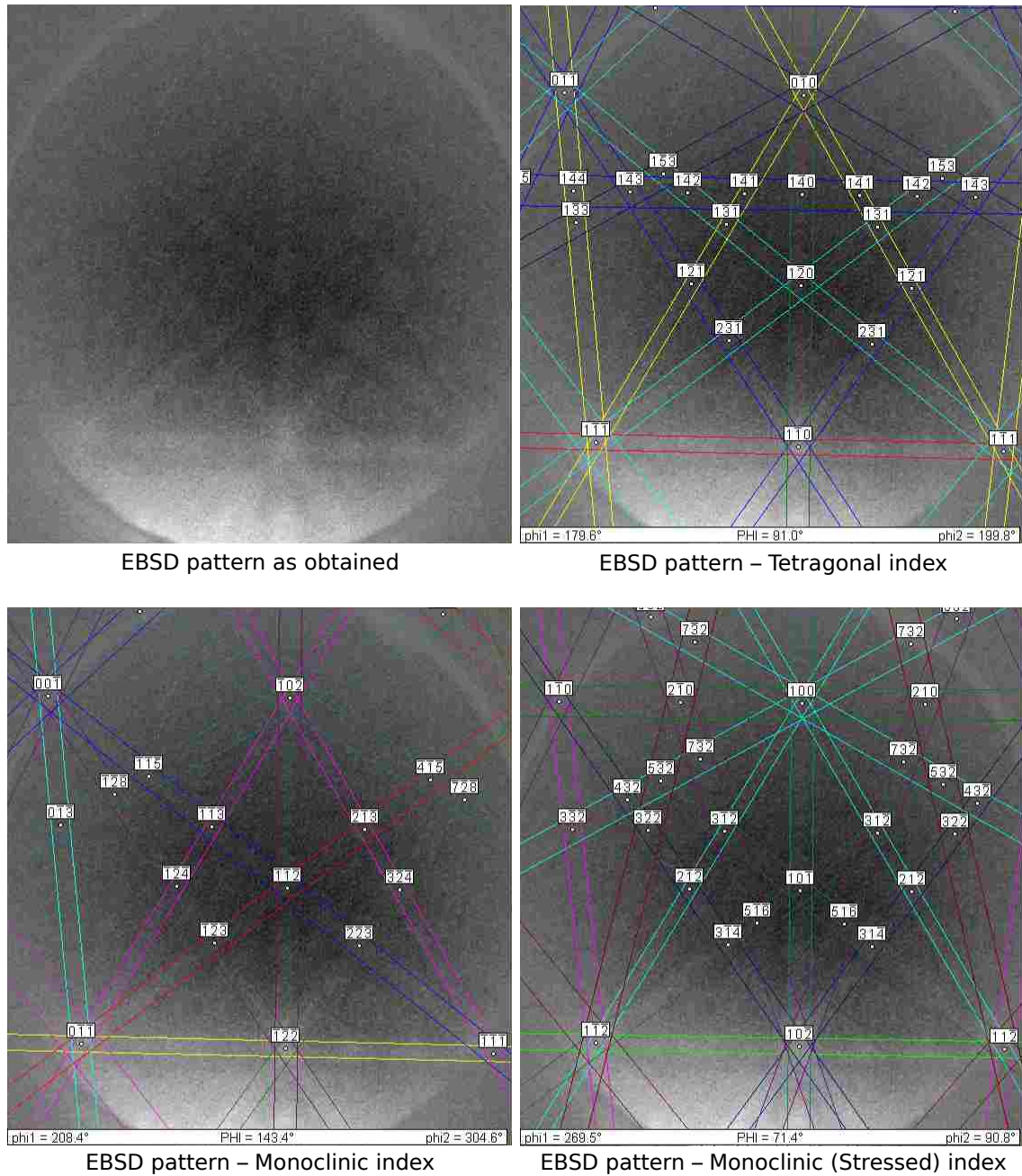
Figure 2.15 Electron Back-Scattered Diffraction Pattern obtained from the sample annealed at 450°C for 17 hrs. Due to the many similarities between the calculated EBSD patterns for the three known vanadium dioxide phases, the software is unable to distinguish between them. The tetragonal index is the most readily recognized and, because of its symmetry, more easily indexed. Also, the grain formation and orientation took place during the annealing at $T > 300°C$ where the structure formed was tetragonal.

2.2.3 Results of the Orientation Imaging Microscopy

Results of the data obtained from the OIM analysis are summarized in figures 2.16, 2.17, and 2.18. These results were obtained from an OIM scan performed on a sample annealed at 450°C for 17 hrs. They are characteristic of the results obtained from all the anneals performed in argon above 440°C where the grains were allowed to grow to the thickness of the film.

Figure 2.16 shows orientation maps compiled from a scan obtained in the manner described in section 2.1.3. The horizontal dimension of the scan is approximately 2 μm and EBSD patterns obtained every 50 nm in a hexagonal grid. Two maps of the same data were generated. They display the orientation of the grains with respect to the Normal Direction. Map A uses 3 colors for the fitted data, while map B weighs the colors (in gray-scale) with the pattern's image quality.

This data was sectioned for 3 different orientations:

1. Grains with the C axis $\langle 001 \rangle$ of the tetragonal phase normal to the plane of the specimen. (Red in maps A, and B) [11]

2. Grains with the A axis $\langle 100 \rangle$ of the tetragonal phase[12] normal to the surface. (Blue in maps A, and B)

3. The $\langle 110 \rangle$ direction of the tetragonal phase normal to the plane of the specimen. (Yellow in map A, and green in map B)

4. Black shows non-indexable patterns (indicative of lack of crystalline material).

The lines separating the grains in Map A are color-coded to indicate the misorientation between the grains.

---

[11]The red coloring is up to and including a 60° deviation from the normal.

[12]in the tetragonal structure, the A and B axes are equivalent

1. Misorientations between 2° and 5° are colored red in map A and yellow in map B.

2. Misorientations between 5° and 15° are colored green in map A and orange in map B.

3. Misorientations between 15° and 180° are colored blue in map A and brown in map B.

Misorientation smaller than 2° are considered part of the same grain.

Figure 2.16 shows in both maps the lack of grains with the $\langle 001 \rangle$ normal to the surface of the specimen.

The orientation of each data point was plotted using Pole Figures (PF).[13] Figure 2.17 shows pole figures for seven crystal directions and their mappings onto the plane of the specimen. The center of the plot is the Normal Direction (ND). The reference and transverse directions are noted (refer to figure 2.12). The crystal directions plotted are the $\langle 001 \rangle$, $\langle 010 \rangle$, $\langle 100 \rangle$, $\langle 101 \rangle$, $\langle 110 \rangle$, $\langle 011 \rangle$, and $\langle 111 \rangle$.[14] The pole figures again show the lack of crystals with the $\langle 001 \rangle$ direction normal to the surface, and an even distribution of the $\langle 001 \rangle$ direction on the plane of the specimen. Similarly, an Inverse Pole Figure (IPF)[15] shows what crystal orientations are parallel to the Normal Direction (ND).[16]

Using this data, the texture of the film can be determined. Figure 2.18 shows pole figures with the texture of a sample annealed at 450°C. The same notation is used as

---

[13]A pole figure is quite similar to a stereographic projection.

[14]In each of the pole figures, the label above the plot indicates which crystal direction is being plotted. The point indicates the orientation of that crystal direction with respect to the coordinates of the sample.

[15]In an IPF, the label for the graph indicates the direction used as a reference with respect to the sample itself. Each data point shows the crystal direction that is parallel to the reference used.

[16]The notation [001] in the IPF refers to the Normal Direction (ND)
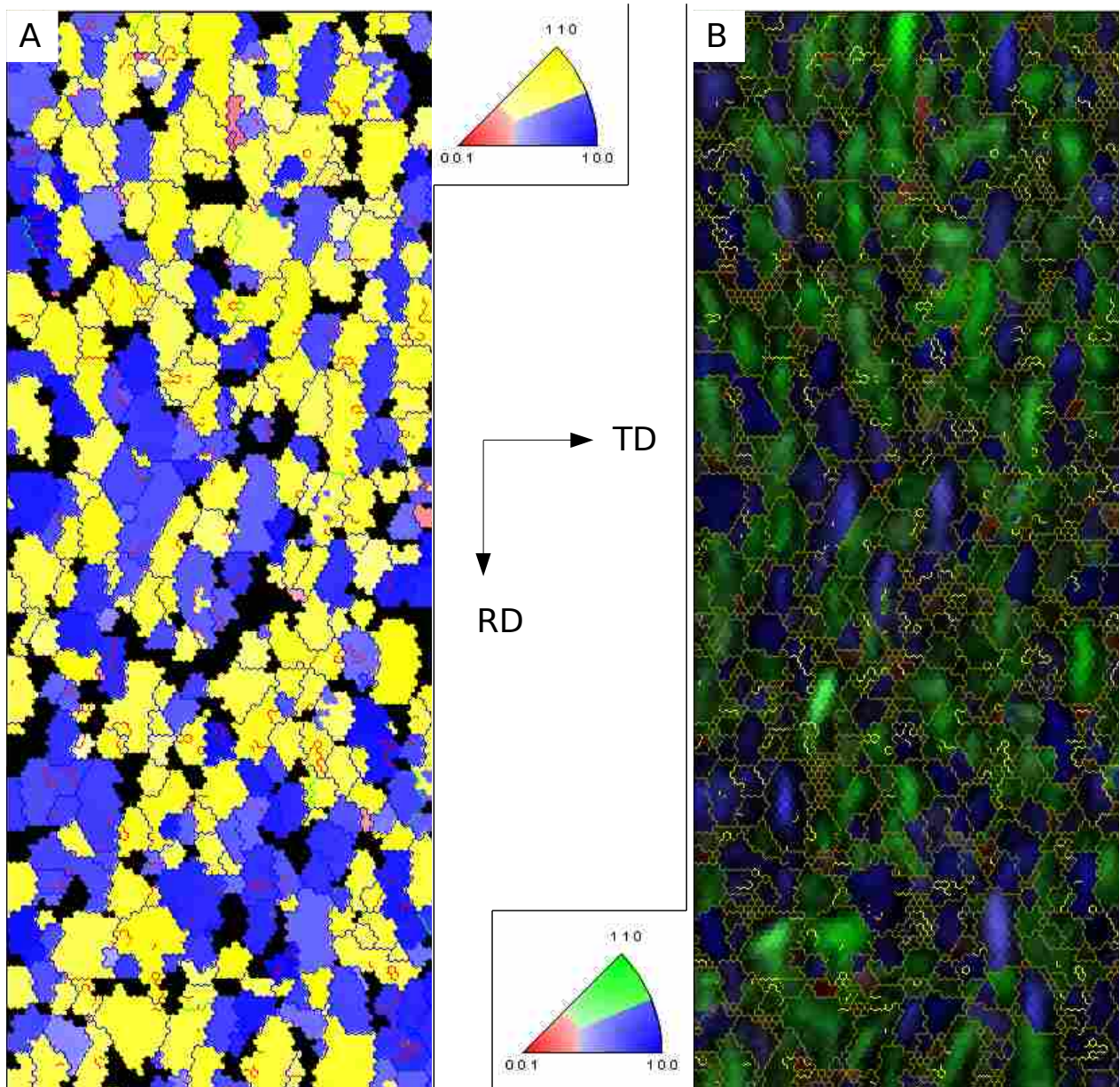
Figure 2.16 [Color] Inverse Pole Figure Map of a scan performed. This image maps out the different crystals scanned and their orientation. Crystal boundaries are determined by the misorientations found within the scan. The boundaries are color-coded depending on the misorientation between data points. Map A shows the overall grains, whereas Map B overlays (in gray-scale) the image quality of each data point obtained.

in figure 2.17. This data shows a preferred orientation of the $\langle 001 \rangle$ crystal direction of the tetragonal phase parallel to the surface of the specimen
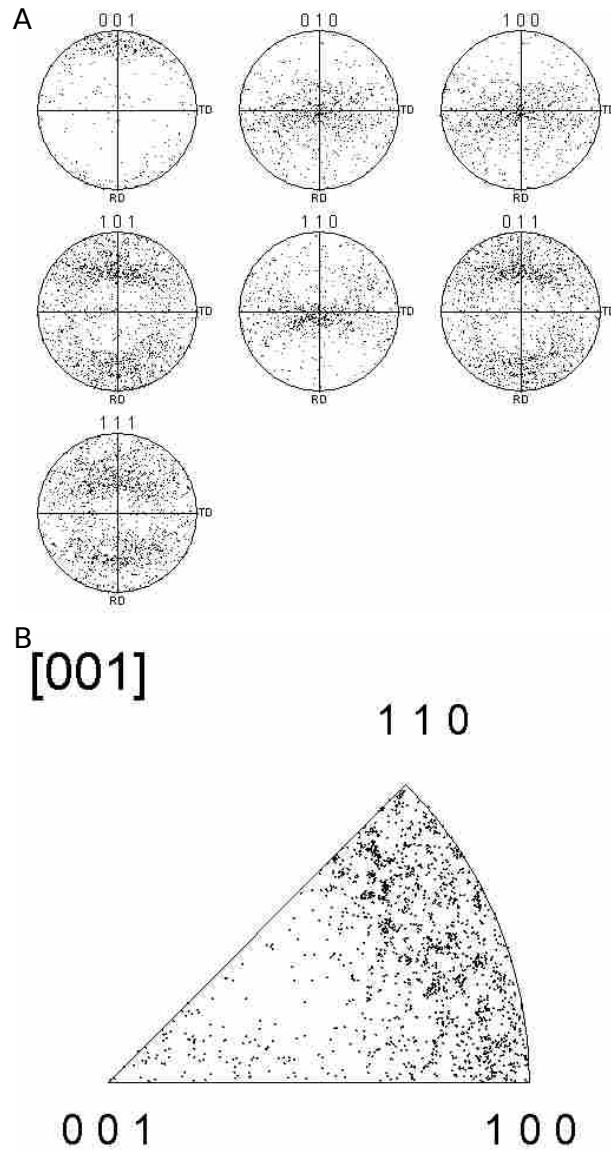
Figure 2.17 Pole Figure (PF) and Inverse Pole Figure (IPF) of an OIM scan obtained from a sample annealed at 450°C. This data is characteristic of the samples annealed above 440°C. Each data point represents the orientation recorded. In the Pole Figure, the Reference Direction (RF) and the Transverse Direction is noted. The index mentioned on top of the pole figure represents the direction normal to the surface of the sample. The Inverse Pole Figure (IPF) shows the orientations normal to the surface. Notice the lack of ⟨001⟩ crystallographic direction absent from the normal to the plane. (This is plot of the raw data)
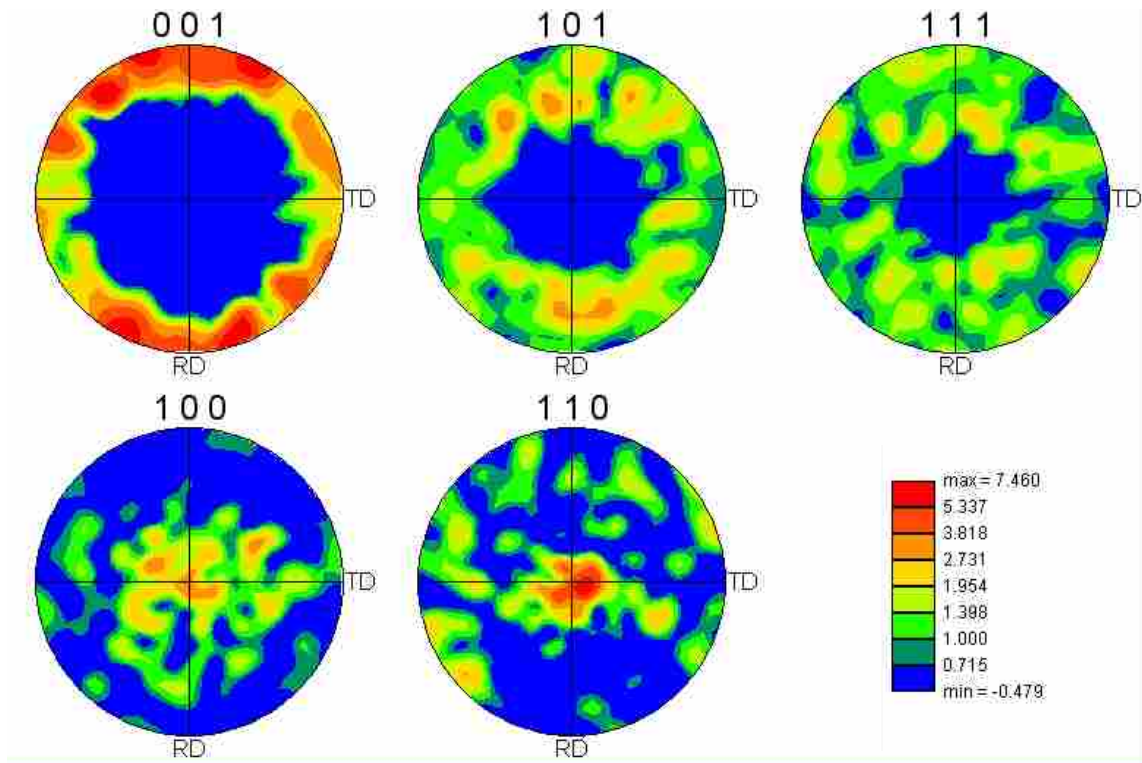
Figure 2.18 Pole Figure (PF) of the texture obtained from a sample annealed at 450°C. In the Pole Figure, the Reference Direction (RF) and the Transverse Direction is noted. The texture shows a preferred orientation of the ⟨001⟩ crystal direction of the tetragonal phase parallel to the surface of the specimen.

2.3   Annealing in an Air Atmosphere

As described in section 2.1.1 annealing under an air atmosphere took place. Similar to the anneals done in argon, no crystallization was observed under 300°C and high mobility was observed at temperatures above 600°C. Figure 2.19 summarizes the results. It was observed that the crystals obtained indexed to the V_2O_5 structure with the anneals as early as 300°C. The presence of air allowed for further oxidation of the VO_2 thin films and formed V_2O_5.
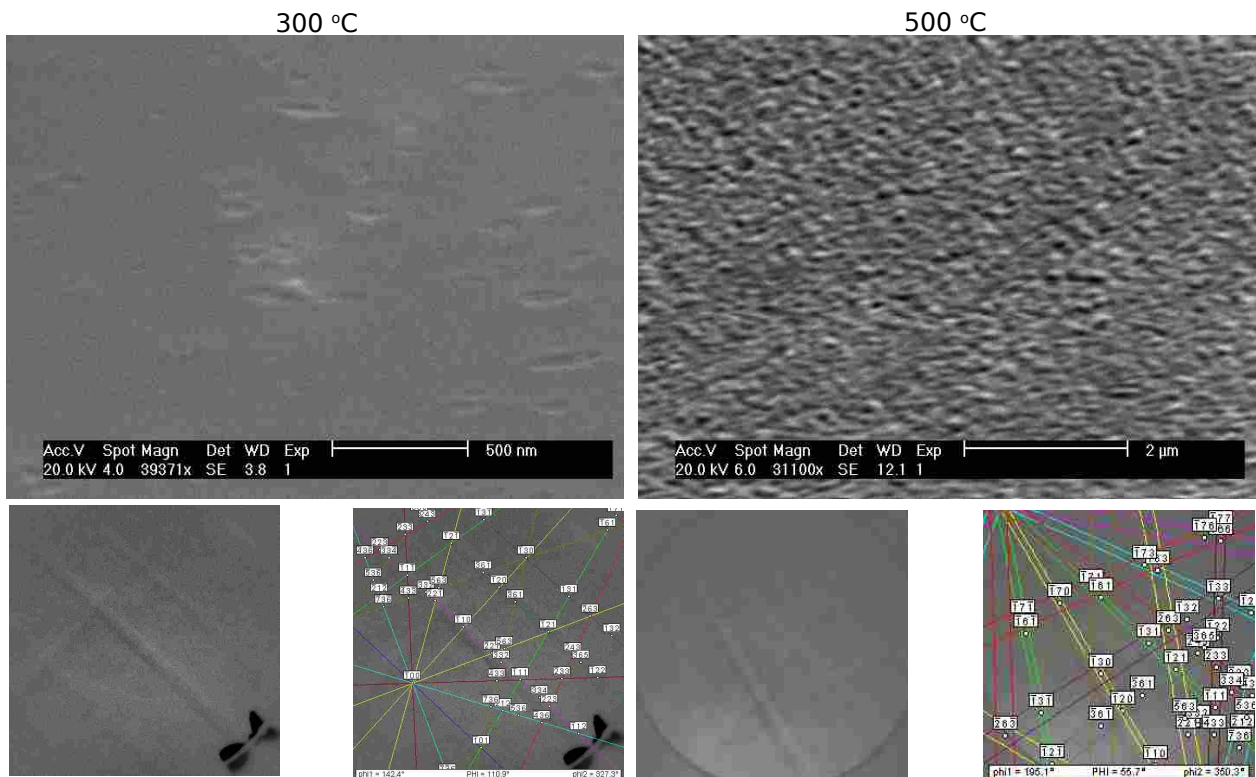
Figure 2.19 Scanning electron micrographs and EBSD patterns collected of two characteristic air anneals. The EBSD patterns show that the resulting films, though crystalline, formed V_2O_5 instead of VO_2.

Chapter 3

Conclusions - Future Work

3.1 Solid Phase Crystallization and Characterization Using Scanning Electron Microscopy

Solid Phase Crystallization of vanadium dioxide thin films was achieved through a thermal anneal process. Depending on the annealing conditions, the processing yielded continuous films, semi-continuous films, and films of isolated particles, all with single-crystal grains. The size of the grains again depended upon the annealing conditions. The grain sizes varied from 50 nm up to 1 μm grain sizes. For the anneals that allowed the grains to grow to the thickness of the film, the vanadium dioxide crystal grains showed a preferred orientation for these crystals with the C axis of the tetragonal phase parallel to the plane of the specimen.[1]

If this material is to be used in electronic, optical, and other technical applications, Orientation Imaging Microscopy is a tool that will allow for a much closer look at the film. This technique may extract detailed information regarding the quality of

---

[1]This information that might prove beneficial for the inclusion of VO_2 in electronic devices, considering the use of SiO_2 as an insulating layer in current electronic fabrication.

a deposited film or individual particles down to submicron-size grains. Information regarding variations in particle size, stress, misorientations between grains, morphological faults, and other imperfections that may affect the transition temperature and hysteresis of deposited vanadium dioxide can be extracted using OIM.

However, it was observed that a crystal size of $\sim$100 nm in length and width, with a $\sim$50 nm thickness was a lower imaging limit for the OIM technique in this study. Another limitation found with this technique was the inability of the software to distinguish between the different phases of vanadium dioxide because the differences in the calculated EBSD patterns are very subtle. Thus this method would not be efficient in observing the phase transition for individual grains in the film.

3.2 Future Work

So far, this thesis presented the use of the tetragonal structure of vanadium dioxide as means of characterizing thin films of crystalline VO_2 inside the Scanning Electron Microscope. However, it was found that there was a limit in size for this technique. Further characterization of the films produced may be carried out by means of Transmission Electron Microscopy (TEM) in order to overcome the size limit[2]. The TEM allows collection of both images and diffraction information from the sample. Thus with the use of the TEM, it will be possible not only to image smaller grains than with the SEM, but also to observe the phase transition due to the structural change that takes place.

The metal to insulator phase transition can also be used to even further study these films. In order to probe individual grains in the film Conductive Atomic Force Microscopy may be employed. There is evidence to show that a change in capacitance

---

[2]Refer to appendix C.1 for current capabilities at BYU

can be observed for individual grains as the transition takes place in the vanadium dioxide films.[3]

Up to the time of this thesis, the nature of the metal to insulator transition of VO_2 still is debated. Different models that attempt to describe the hysteresis observed in the transition assume behavior of individual particles based on large ensembles of particles in films. Hopefully, future work in the observation of the metal to insulator transition of individual nanoparticles will help clarify the models currently used, and perhaps will also shed light on the nature of the transition itself.

---

[3]For work currently underway at the time of this thesis, the reader is encouraged to refer t appendix. C

Appendix A

Deposition Parameters of the Amorphous VO$_x$ Film

The VO$_x$ film obtained for this work was obtained from Kevin Coffey at the University of Central Florida. The film was deposited by means of Reactive RF Magnetron Sputtering.

- Sample#050506

- 0.5% oxygen partial pressure.

- 8min deposition time

- RF power: 260 V and 40 W

- DC power: 200 W

- DC voltage: 334 V

- DC current: 0.595 amps

The substrate was a silicon wafer with a thermally grown amorphous silicon dioxide layer approximately 380 nm in thickness, and the resulting VO_x film was approximately 50 nm

Appendix B

Use of ISODISPLACE to Model the Phase Transition

ISODISPLACE is a web-based tool that enables the study of structural phase transitions. It can be used via a web-browser and allows the user to visualize and manipulate the transition. *ISODISPLACE* uses subroutines available in the *ISOTROPY*[1] software package and wraps an easy to use graphical user interface. [28]

In order to use *ISODISPLACE* the two phases must be introduced. Then, the software decomposes the phase transition by:

1. Determining the distortion symmetry

2. Identifying the distortion modes

3. Determining the individual mode amplitudes

4. Expressing the distorted structure in terms of the familiar xyz basis

Once a distortion has been computed, an interactive Java applet shows a three-dimensional image of how the two structures match. These representations shows how

---

[1]This software package is available at http://stokes.byu.edu/isotropy.html [43]

the shapes of the structures, lattice parameters, atomic bonds, and atom positions change during the phase transition. Futher, the applet also allows for:

1. Specific viewing directions

2. Rotations of the structures

3. Zooming

4. Animating the phase transition

5. Adjusting each distortion individually

Thus making it easier to visualize how the phase transition takes place. *ISODIS-PLACE* is currently available at http://stokes.byu.edu/isodisplace.html [28]

B.1 Phase Transition of Vanadium Dioxide Between the Rutile (R) phase and the Monoclinic (M3) Phase

Figure B.1 shows the rutile structure (in pink) and the monoclinic $M3$ structure (in blue) as well as each of the atom positions. The $M3$ structure is four times as big as the R structure due to the doubling of two of the basis vectors of the R structure.

Figure B.2. shows the changes observed looking down the a, b, and c axis of the tetragonal phase. The displacement of the vanadium atoms is evident in views A and C by looking at the vanadium-oxygen bonds. View B shows a "bowing" that takes place in the $M3$ phase. *ISODISPLACE* shows that the phase transition between the R and the $M3$ phase produces a slight change in the angle (seen in view C) from 90° to 91.8°.
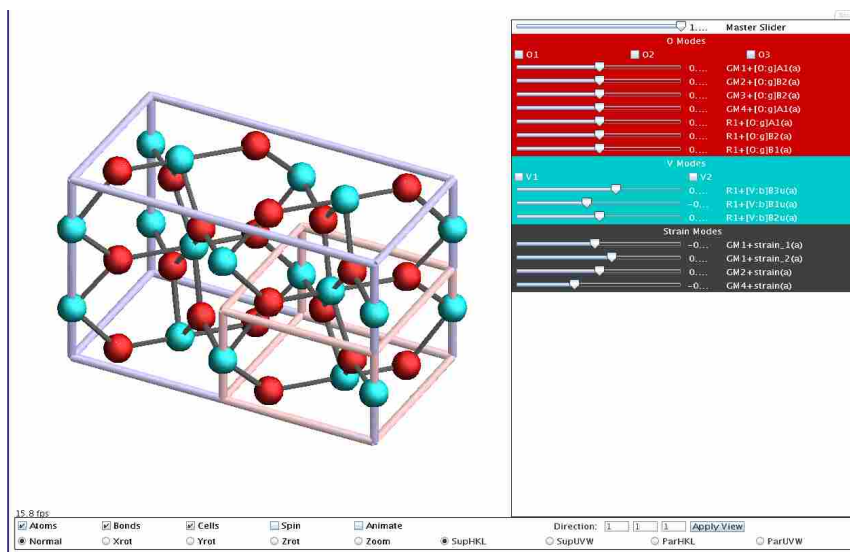
Figure B.1 *ISODISPLACE* showing the monoclinic, $M3$ (blue), and the
tetragonal, R (pink), structures for vanadium dioxide. The doubling of two
basis vectors is evident from the diagram. Vanadium atoms are shown in
cyan while the oxygen atoms are shown in red.

B.1.1 Distortion File for the Phase Transition of Vanadium Dioxide Between the Rutile (R) phase and the Monoclinic (M3) Phase

The following file is generated by *ISODISPLACE* saving the required information
that the Java applet needs to show the phase transition. Some of the code saved
is intended to be displayed as choices in the web browser, and options that will be
passed on to applet itself. However, the changes that take place during the transition
are also stored in the file itself. Some of the information stored which regards to the
phase transition includes:

1. The "high-symmetry" rutile structure [2] (including the lattice parameters, space-
   group, and the atom positions)

---

[2]This structure is also known as the "parent" structure.

A.

B.

C.

Tetragonal (R) Phase   Monoclinic (M3) Phase
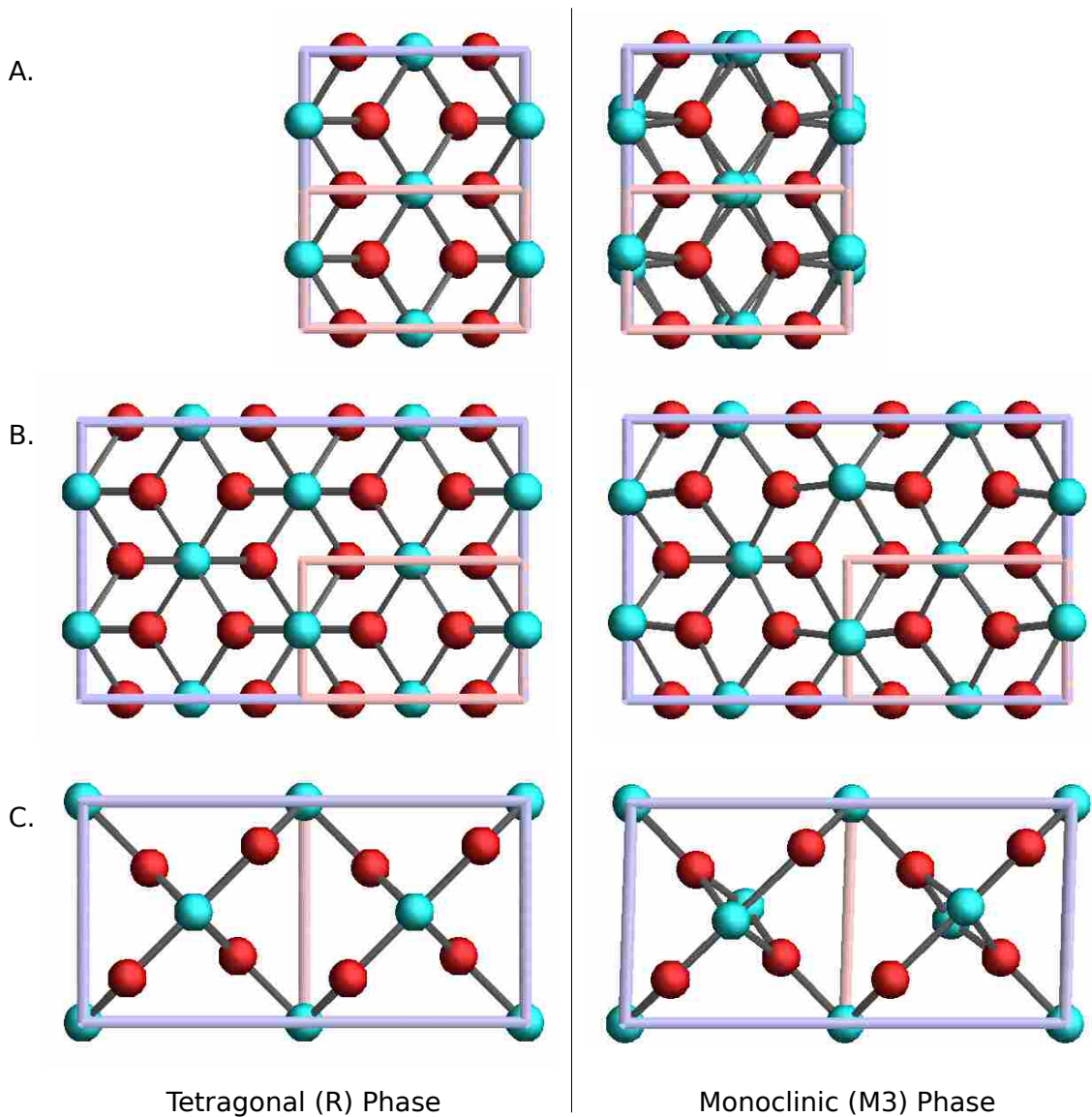
Figure B.2 The changes observed with *ISODISPLACE* showing the changes between the $M3$ and the R structures for vanadium dioxide. The three views in A, B, and C correspond to viewing down the a, b, and c axis of the tetragonal phase (respectively). The displacement of the vanadium atoms is evident in A and C from the vanadium-oxygen bonds. C also shows a change in angle that takes place during the phase transition. Vanadium atoms are shown in cyan while the oxygen atoms are shown in red.

2. Specific changes to the unit cell (including the magnitude of each change)

3. Specific changes to the atom positions (also including the magnitude of the change)

4. Whether the transition is first order or continuous.

This text may be copied into a ".txt" file and uploaded into *ISODISPLACE* in order to view the model of the transition.

```
Space Group: 136 P4_2/mnm   D4h-14,
Lattice parameters: a=4.55460, b=4.55460, c=2.85140, alpha=90.00000, beta=90.00000, gamma=90.00000<br>
Space-group preferences: monoclinic axes a(b)c, monoclinic cell choice 1, orthorhombic axes abc, origin choice 1, hexagonal axes<br>
O 4f   (x,x,0), x= 0.30000,
V 2a   (0,0,0)<br>
Subgroup:  12 C2/m, basis={(0,2,0),(0,0,2),(1,0,0)}, origin=(0,0,1/2), s=2, i=8<br>
<FORM ACTION="isodisplace2.cgi" METHOD="POST" target="_blank">
<INPUT TYPE="hidden" NAME="input" VALUE="displaydistort">
<INPUT TYPE="hidden" NAME="spacegroup" VALUE="136 P4_2/mnm   D4h-14">
<INPUT TYPE="hidden" NAME="settingaxesm" VALUE="a(b)c            ">
<INPUT TYPE="hidden" NAME="settingcell" VALUE="1">
<INPUT TYPE="hidden" NAME="settingorigin" VALUE="1">
<INPUT TYPE="hidden" NAME="settingaxesh" VALUE="h">
<INPUT TYPE="hidden" NAME="settingaxeso" VALUE="abc             ">
<INPUT TYPE="hidden" NAME="lattparam" VALUE="a=4.55460, b=4.55460, c=2.85140, alpha=90.00000, beta=90.00000, gamma=90.00000">
<INPUT TYPE="hidden" NAME="dlattparam" VALUE="   4.5546      4.5546      2.8514       90.00       90.00       90.00">
<INPUT TYPE="hidden" NAME="wycount" VALUE="  2">
<INPUT TYPE="hidden" NAME="wypointer001" VALUE="1004">
<INPUT TYPE="hidden" NAME="wynumber001" VALUE=" 6">
<INPUT TYPE="hidden" NAME="wyckoff001" VALUE="4f   (x,x,0), x= 0.30000">
<INPUT TYPE="hidden" NAME="wyatom001" VALUE="O">
<INPUT TYPE="hidden" NAME="wyparam001" VALUE=" 0.300000000000000       0.000000000000000E+000  0.000000000000000E+000">
<INPUT TYPE="hidden" NAME="wypointer002" VALUE=" 999">
<INPUT TYPE="hidden" NAME="wynumber002" VALUE=" 1">
<INPUT TYPE="hidden" NAME="wyckoff002" VALUE="2a   (0,0,0)">
<INPUT TYPE="hidden" NAME="wyatom002" VALUE="V">
<INPUT TYPE="hidden" NAME="wyparam002" VALUE=" 0.000000000000000E+000  0.000000000000000E+000  0.000000000000000E+000">
<INPUT TYPE="hidden" NAME="irrepcount" VALUE="0">
<INPUT TYPE="hidden" NAME="basisorigin" VALUE="   1   0   0   0   1   1   0  -1   1   0   0   1   2">
<INPUT TYPE="hidden" NAME="isofilename" VALUE="             ">
<INPUT TYPE="hidden" NAME="orderparam" VALUE="Subgroup:  12 C2/m, basis={(0,2,0),(0,0,2),(1,0,0)}, origin=(0,0,1/2), s=2, i=8">
<INPUT TYPE="hidden" NAME="isosubgroup" VALUE="    0">
<INPUT TYPE="hidden" NAME="subgroupsym" VALUE="  12">
<INPUT TYPE="hidden" NAME="distortfilename" VALUE="isodisplac3_16707.iso">
<INPUT TYPE="hidden" NAME="atomsfilename" VALUE="isodisplace_55267.iso">
<p><INPUT TYPE="radio" NAME="origintype" VALUE="viewdistortion" CHECKED> View distortion
<a href="/iso/isodisplacehelp.html#viewdist" target="_blank">(help)</a>
<INPUT TYPE="radio" NAME="origintype" VALUE="viewdiffraction"> View diffraction
<a href="/iso/isodisplacehelp.html#viewdiff" target="_blank">(help)</a>
<INPUT TYPE="radio" NAME="origintype" VALUE="structurefile"> CIF file
<a href="/iso/isodisplacehelp.html#cifsub" target="_blank">(help)</a>
<INPUT TYPE="radio" NAME="origintype" VALUE="distortionfile"> Distortion file
<a href="/iso/isodisplacehelp.html#dfile" target="_blank">(help)</a>
<INPUT TYPE="radio" NAME="origintype" VALUE="domains"> Domains
<a href="/iso/isodisplacehelp.html#domains" target="_blank">(help)</a>
<INPUT TYPE="radio" NAME="origintype" VALUE="primary"> Primary order parameters
<a href="/iso/isodisplacehelp.html#setsprimary" target="_blank">(help)</a>
<INPUT TYPE="submit" VALUE="OK"><p>
Enter mode and strain amplitudes:
<a href="/iso/isodisplacehelp.html#modeamp" target="_blank">(help)</a><br>
<p>
P4_2/mnm[0,0,0]GM1+(a) 136 P4_2/mnm, basis={(1,0,0),(0,1,0),(0,0,1)}, origin=(0,0,0), s=1 i=1<br>
<input type="text" name="mode001001" value="  -0.02834" size=5>[O:f]A1(a)<br>
<input type="text" name="strain1" value="  -0.00554" size=5>strain_1(a)<br>
<input type="text" name="strain2" value="   0.01652" size=5>strain_2(a)<br>
<p>
P4_2/mnm[0,0,0]GM2+(a) 58 Pnnm, basis={(1,0,0),(0,1,0),(0,0,1)}, origin=(0,0,0), s=1 i=2<br>
<input type="text" name="mode001002" value="  -0.00676" size=5>[O:f]B1(a)<br>
<input type="text" name="strain3" value="  -0.00085" size=5>strain(a)<br>
<p>
P4_2/mnm[0,0,0]GM3+(a) 84 P4_2/m, basis={(0,1,0),(-1,0,0),(0,0,1)}, origin=(0,1/2,0), s=1 i=2<br>
<input type="text" name="mode001003" value="  -0.00032" size=5>[O:f]B1(a)<br>
<p>
P4_2/mnm[0,0,0]GM4+(a) 65 Cmmm, basis={(-1,1,0),(-1,-1,0),(0,0,1)}, origin=(0,0,0), s=1 i=2<br>
```

```
<input type="text" name="mode001004" value="  -0.00193" size=5>[O:f]A1(a)<br>
<input type="text" name="scalar001001" value="   0.00000" size=5>[O:f]order(a)<br>
<input type="text" name="scalar002001" value="   0.00000" size=5>[V:a]order(a)<br>
<input type="text" name="strain4" value="  -0.03281" size=5>strain(a)<br>
<p>
P4_2/mnm[0,1/2,1/2]R1-(0,a,0,0) 12 C2/m, basis={(0,2,0),(0,0,2),(1,0,0)}, origin=(0,0,1/2), s=2 i=8<br>
<input type="text" name="mode001005" value="  -0.02222" size=5>[O:f]A1(a)<br>
<input type="text" name="mode001006" value="   0.01426" size=5>[O:f]B2(a)<br>
<input type="text" name="mode001007" value="   0.00225" size=5>[O:f]B1(a)<br>
<input type="text" name="mode002001" value="  -0.22029" size=5>[V:a]B3u(a)<br>
<input type="text" name="mode002002" value="  -0.17736" size=5>[V:a]B1u(a)<br>
<input type="text" name="mode002003" value="  -0.01932" size=5>[V:a]B2u(a)<br>
<input type="text" name="scalar001002" value="   0.00000" size=5>[O:f]order(a)<br>
<p>Parameters:
<a href="/iso/isodisplacehelp.html#modeparams" target="_blank">(help)</a><br>
"View distortion":<br>
Atomic radius:
<input type="text" name="atomicradius" value="      0.400" size=5> Angstroms<br>
Maximum bond length:
<input type="text" name="bondlength" value="      2.114" size=5> Angstroms<br>
Applet width:
<input type="text" name="appletwidth" value="1024" size=5> pixels<br>
"View distortion" and "View diffraction":<br>
Maximum mode amplitudes:
<input type="text" name="modeamplitude" value="      1.000" size=5> Angstroms<br>
Maximum strain amplitudes:
<input type="text" name="strainamplitude" value="      0.100" size=5><p>
</FORM><p>
<A href="/iso/isodisplacehelp.html" target="_blank"><B>Complete help file</B></A><P>
distortfilename=isodisplac3_16707.iso
        20          7          2          5         16          8
        20         18          7          3          2          1
         3          2          4
      6454       6455       6456       6457       6490          0
         0          0          0          0          0          0
         0          0          0          0          0          0
         0          0          0          0          0          0
         0        136         58         84         65         12
         1          1          1          1          2          1
         2          2          2          8          1          2
         3          4          5          5          5          5
         5          5        396        399        399        396
       396        398        399        781        780        782
         4          5          4        396        396        775
         1          1          2          4          1          1
         1          1          4          1          1          1
         1          1
         1          0          0          0          1          0
         0          0          1          0          0          0
         1
         1          0          0          0          1          0
         0          0          1          0          0          0
         1
         0          1          0         -1          0          0
         0          0          1          0          1          0
         2
         0          1          0         -1          0          0
         0          0          1          0          0          0
         1
         1          0          0          0          1          1
         0         -1          1          0          0          1
         2
   9.10920000   5.70280000   4.55460000  90.00000000  90.00000000  90.00000000
   0.50000000   0.25000000   0.00000000   0.00000000   0.00000000   1.00000000
   0.50000000   0.00000000   0.00000000   0.00000000   0.50000000   0.00000000
   1.92150227
   1.00000000   1.00000000   0.00000000   0.00000000   0.00000000   0.00000000
   0.00000000   0.00000000   1.00000000   0.00000000   0.00000000   0.00000000
   1.00000000  -1.00000000   0.00000000   0.00000000   0.00000000   0.00000000
   0.00000000   0.00000000   0.00000000   0.00000000   0.00000000   1.00000000
   1.00000000   1.00000000   1.00000000   1.00000000   0.00000000   1.00000000
   0.00000000   0.00000000
   1   0.150000000000   0.750000000000   0.300000000000   0.077625563297
       0.000000000000   0.155251126594  -0.077625563297   0.000000000000
       0.155251126594  -0.077625563297   0.000000000000   0.155251126594
       0.077625563297   0.000000000000   0.155251126594   0.000000000000
       0.000000000000   0.000000000000   0.000000000000   0.175352458441
       0.000000000000   0.000000000000   0.000000000000   0.000000000000
       1.000000000000   0.000000000000
   1   0.150000000000   0.250000000000   0.300000000000   0.077625563297
       0.000000000000   0.155251126594  -0.077625563297   0.000000000000
       0.155251126594  -0.077625563297   0.000000000000   0.155251126594
       0.077625563297   0.000000000000   0.155251126594   0.000000000000
       0.000000000000   0.000000000000   0.000000000000  -0.175352458441
       0.000000000000   0.000000000000   0.000000000000   0.000000000000
       1.000000000000   0.000000000000
   1   0.650000000000   0.750000000000   0.300000000000   0.077625563297
       0.000000000000   0.155251126594  -0.077625563297   0.000000000000
```

```
      0.155251126594  -0.077625563297   0.000000000000   0.155251126594
      0.077625563297   0.000000000000   0.155251126594   0.000000000000
      0.000000000000   0.000000000000   0.000000000000  -0.175352458441
      0.000000000000   0.000000000000   0.000000000000   0.000000000000
      1.000000000000   0.000000000000
1     0.650000000000   0.250000000000   0.300000000000   0.077625563297
      0.000000000000   0.155251126594  -0.077625563297   0.000000000000
      0.155251126594  -0.077625563297   0.000000000000   0.155251126594
      0.077625563297   0.000000000000   0.155251126594   0.000000000000
      0.000000000000   0.000000000000   0.000000000000   0.175352458441
      0.000000000000   0.000000000000   0.000000000000   0.000000000000
      1.000000000000   0.000000000000
2     0.100000000000   0.000000000000   0.800000000000  -0.077625563297
      0.000000000000   0.155251126594   0.077625563297   0.000000000000
      0.155251126594  -0.077625563297   0.000000000000  -0.155251126594
      0.077625563297   0.000000000000  -0.155251126594   0.077625563297
      0.000000000000  -0.155251126594   0.000000000000   0.000000000000
      0.000000000000   0.077625563297   0.000000000000   0.155251126594
     -1.000000000000  -1.000000000000
3     0.100000000000   0.500000000000   0.800000000000  -0.077625563297
      0.000000000000   0.155251126594   0.077625563297   0.000000000000
      0.155251126594  -0.077625563297   0.000000000000  -0.155251126594
      0.077625563297   0.000000000000  -0.155251126594  -0.077625563297
      0.000000000000   0.155251126594   0.000000000000   0.000000000000
      0.000000000000  -0.077625563297   0.000000000000  -0.155251126594
     -1.000000000000   1.000000000000
3     0.600000000000   0.000000000000   0.800000000000  -0.077625563297
      0.000000000000   0.155251126594   0.077625563297   0.000000000000
      0.155251126594  -0.077625563297   0.000000000000  -0.155251126594
      0.077625563297   0.000000000000  -0.155251126594  -0.077625563297
      0.000000000000   0.155251126594   0.000000000000   0.000000000000
      0.000000000000  -0.077625563297   0.000000000000  -0.155251126594
     -1.000000000000   1.000000000000
2     0.600000000000   0.500000000000   0.800000000000  -0.077625563297
      0.000000000000   0.155251126594   0.077625563297   0.000000000000
      0.155251126594  -0.077625563297   0.000000000000  -0.155251126594
      0.077625563297   0.000000000000  -0.155251126594   0.077625563297
      0.000000000000  -0.155251126594   0.000000000000   0.000000000000
      0.000000000000   0.077625563297   0.000000000000   0.155251126594
     -1.000000000000  -1.000000000000
3     0.400000000000   0.000000000000   0.200000000000   0.077625563297
      0.000000000000  -0.155251126594  -0.077625563297   0.000000000000
     -0.155251126594   0.077625563297   0.000000000000   0.155251126594
     -0.077625563297   0.000000000000   0.155251126594   0.077625563297
      0.000000000000  -0.155251126594   0.000000000000   0.000000000000
      0.000000000000   0.077625563297   0.000000000000   0.155251126594
     -1.000000000000   1.000000000000
2     0.400000000000   0.500000000000   0.200000000000   0.077625563297
      0.000000000000  -0.155251126594  -0.077625563297   0.000000000000
     -0.155251126594   0.077625563297   0.000000000000   0.155251126594
     -0.077625563297   0.000000000000   0.155251126594  -0.077625563297
      0.000000000000   0.155251126594   0.000000000000   0.000000000000
      0.000000000000  -0.077625563297   0.000000000000  -0.155251126594
     -1.000000000000  -1.000000000000
2     0.900000000000   0.000000000000   0.200000000000   0.077625563297
      0.000000000000  -0.155251126594  -0.077625563297   0.000000000000
     -0.155251126594   0.077625563297   0.000000000000   0.155251126594
     -0.077625563297   0.000000000000   0.155251126594  -0.077625563297
      0.000000000000   0.155251126594   0.000000000000   0.000000000000
      0.000000000000  -0.077625563297   0.000000000000  -0.155251126594
     -1.000000000000  -1.000000000000
3     0.900000000000   0.500000000000   0.200000000000   0.077625563297
      0.000000000000  -0.155251126594  -0.077625563297   0.000000000000
     -0.155251126594   0.077625563297   0.000000000000   0.155251126594
     -0.077625563297   0.000000000000   0.155251126594   0.077625563297
      0.000000000000  -0.155251126594   0.000000000000   0.000000000000
      0.000000000000   0.077625563297   0.000000000000   0.155251126594
     -1.000000000000   1.000000000000
1     0.850000000000   0.750000000000   0.700000000000  -0.077625563297
      0.000000000000  -0.155251126594   0.077625563297   0.000000000000
     -0.155251126594   0.077625563297   0.000000000000  -0.155251126594
     -0.077625563297   0.000000000000  -0.155251126594   0.000000000000
      0.000000000000   0.000000000000   0.000000000000   0.175352458441
      0.000000000000   0.000000000000   0.000000000000   0.000000000000
      1.000000000000   0.000000000000
1     0.850000000000   0.250000000000   0.700000000000  -0.077625563297
      0.000000000000  -0.155251126594   0.077625563297   0.000000000000
     -0.155251126594   0.077625563297   0.000000000000  -0.155251126594
     -0.077625563297   0.000000000000  -0.155251126594   0.000000000000
      0.000000000000   0.000000000000   0.000000000000  -0.175352458441
      0.000000000000   0.000000000000   0.000000000000   0.000000000000
      1.000000000000   0.000000000000
1     0.350000000000   0.750000000000   0.700000000000  -0.077625563297
      0.000000000000  -0.155251126594   0.077625563297   0.000000000000
     -0.155251126594   0.077625563297   0.000000000000  -0.155251126594
     -0.077625563297   0.000000000000  -0.155251126594   0.000000000000
      0.000000000000   0.000000000000   0.000000000000  -0.175352458441
      0.000000000000   0.000000000000   0.000000000000   0.000000000000
```

```
     1.000000000000    0.000000000000
1    0.350000000000    0.250000000000    0.700000000000   -0.077625563297
     0.000000000000   -0.155251126594    0.077625563297    0.000000000000
    -0.155251126594    0.077625563297    0.000000000000   -0.155251126594
    -0.077625563297    0.000000000000   -0.155251126594    0.000000000000
     0.000000000000    0.000000000000    0.000000000000    0.175352458441
     0.000000000000    0.000000000000    0.000000000000    0.000000000000
     1.000000000000    0.000000000000
2    0.100000000000    1.000000000000    0.800000000000   -0.077625563297
     0.000000000000    0.155251126594    0.077625563297    0.000000000000
     0.155251126594   -0.077625563297    0.000000000000   -0.155251126594
     0.077625563297    0.000000000000   -0.155251126594    0.077625563297
     0.000000000000   -0.155251126594    0.000000000000    0.000000000000
     0.000000000000    0.077625563297    0.000000000000    0.155251126594
    -1.000000000000   -1.000000000000
3    0.600000000000    1.000000000000    0.800000000000   -0.077625563297
     0.000000000000    0.155251126594    0.077625563297    0.000000000000
     0.155251126594   -0.077625563297    0.000000000000   -0.155251126594
     0.077625563297    0.000000000000   -0.155251126594   -0.077625563297
     0.000000000000    0.155251126594    0.000000000000    0.000000000000
     0.000000000000   -0.077625563297    0.000000000000   -0.155251126594
    -1.000000000000    1.000000000000
3    0.400000000000    1.000000000000    0.200000000000    0.077625563297
     0.000000000000   -0.155251126594   -0.077625563297    0.000000000000
    -0.155251126594    0.077625563297    0.000000000000    0.155251126594
    -0.077625563297    0.000000000000    0.155251126594    0.077625563297
     0.000000000000   -0.155251126594    0.000000000000    0.000000000000
     0.000000000000    0.077625563297    0.000000000000    0.155251126594
    -1.000000000000    1.000000000000
2    0.900000000000    1.000000000000    0.200000000000    0.077625563297
     0.000000000000   -0.155251126594   -0.077625563297    0.000000000000
    -0.155251126594    0.077625563297    0.000000000000    0.155251126594
    -0.077625563297    0.000000000000    0.155251126594   -0.077625563297
     0.000000000000    0.155251126594    0.000000000000    0.000000000000
     0.000000000000   -0.077625563297    0.000000000000   -0.155251126594
    -1.000000000000   -1.000000000000
1    0.000000000000    0.750000000000    0.000000000000    0.000000000000
     0.000000000000    0.000000000000    0.000000000000    0.175352458441
     0.000000000000    0.000000000000    0.000000000000    0.000000000000
     1.000000000000
1    0.000000000000    0.250000000000    0.000000000000    0.000000000000
     0.000000000000    0.000000000000    0.000000000000   -0.175352458441
     0.000000000000    0.000000000000    0.000000000000    0.000000000000
     1.000000000000
1    0.500000000000    0.750000000000    0.000000000000    0.000000000000
     0.000000000000    0.000000000000    0.000000000000   -0.175352458441
     0.000000000000    0.000000000000    0.000000000000    0.000000000000
     1.000000000000
1    0.500000000000    0.250000000000    0.000000000000    0.000000000000
     0.000000000000    0.000000000000    0.000000000000    0.175352458441
     0.000000000000    0.000000000000    0.000000000000    0.000000000000
     1.000000000000
2    0.250000000000    0.000000000000    0.500000000000    0.077625563297
     0.000000000000   -0.155251126594    0.000000000000    0.000000000000
     0.000000000000    0.077625563297    0.000000000000    0.155251126594
    -1.000000000000
2    0.250000000000    0.500000000000    0.500000000000   -0.077625563297
     0.000000000000    0.155251126594    0.000000000000    0.000000000000
     0.000000000000   -0.077625563297    0.000000000000   -0.155251126594
    -1.000000000000
2    0.750000000000    0.000000000000    0.500000000000   -0.077625563297
     0.000000000000    0.155251126594    0.000000000000    0.000000000000
     0.000000000000   -0.077625563297    0.000000000000   -0.155251126594
    -1.000000000000
2    0.750000000000    0.500000000000    0.500000000000    0.077625563297
     0.000000000000   -0.155251126594    0.000000000000    0.000000000000
     0.000000000000    0.077625563297    0.000000000000    0.155251126594
    -1.000000000000
1    0.000000000000    0.750000000000    1.000000000000    0.000000000000
     0.000000000000    0.000000000000    0.000000000000    0.175352458441
     0.000000000000    0.000000000000    0.000000000000    0.000000000000
     1.000000000000
1    1.000000000000    0.750000000000    0.000000000000    0.000000000000
     0.000000000000    0.000000000000    0.000000000000    0.175352458441
     0.000000000000    0.000000000000    0.000000000000    0.000000000000
     1.000000000000
1    1.000000000000    0.750000000000    1.000000000000    0.000000000000
     0.000000000000    0.000000000000    0.000000000000    0.175352458441
     0.000000000000    0.000000000000    0.000000000000    0.000000000000
     1.000000000000
1    0.000000000000    0.250000000000    1.000000000000    0.000000000000
     0.000000000000    0.000000000000    0.000000000000   -0.175352458441
     0.000000000000    0.000000000000    0.000000000000    0.000000000000
     1.000000000000
1    1.000000000000    0.250000000000    0.000000000000    0.000000000000
     0.000000000000    0.000000000000    0.000000000000   -0.175352458441
     0.000000000000    0.000000000000    0.000000000000    0.000000000000
     1.000000000000
```

```
   1   1.000000000000    0.250000000000    1.000000000000    0.000000000000
       0.000000000000    0.000000000000    0.000000000000   -0.175352458441
       0.000000000000    0.000000000000    0.000000000000    0.000000000000
       1.000000000000
   1   0.500000000000    0.750000000000    1.000000000000    0.000000000000
       0.000000000000    0.000000000000    0.000000000000   -0.175352458441
       0.000000000000    0.000000000000    0.000000000000    0.000000000000
       1.000000000000
   1   0.500000000000    0.250000000000    1.000000000000    0.000000000000
       0.000000000000    0.000000000000    0.000000000000    0.175352458441
       0.000000000000    0.000000000000    0.000000000000    0.000000000000
       1.000000000000
   2   0.250000000000    1.000000000000    0.500000000000    0.077625563297
       0.000000000000   -0.155251126594    0.000000000000    0.000000000000
       0.000000000000    0.077625563297    0.000000000000    0.155251126594
      -1.000000000000
   2   0.750000000000    1.000000000000    0.500000000000   -0.077625563297
       0.000000000000    0.155251126594    0.000000000000    0.000000000000
       0.000000000000   -0.077625563297    0.000000000000   -0.155251126594
      -1.000000000000
done
atomsfilename=isodisplace_55267.iso
   9.06640    5.79700    4.52550   90.00000   91.88000   90.00000
   0.00000    0.00000    0.00000    0.00000    0.00000    0.00000
O1
   0.14820    0.24750    0.29420
   0.00000    0.00000    0.00000
O2
   0.39690    0.00000    0.20890
   0.00000    0.00000    0.00000
O3
   0.10000    0.00000    0.79870
   0.00000    0.00000    0.00000
V1
   0.00000    0.71890    0.00000
   0.00000    0.00000    0.00000
V2
   0.23140    0.00000    0.53120
   0.00000    0.00000    0.00000
   0.00000    0.00000    0.00000
done
```

Appendix C

Equipment Available for Further Characterization

C.1 TEM Use

The Physics and Astronomy Department at Brigham Young University is equipped with two Transmission Electron Microscopes: The Technai TF30 (a 300 kV, Field-Emission, High Resolution, Transmission Electron Microscope), and the Technai TF20 (a 200 kV Field-Emission, High Resolution, Scanning, Analytical, Transmission Electron Microscope). With the use of these TEMs it is possible to image and obtain information about the deposited films down to individual nano-particles. Furthermore, the analytical capabilities of the TF20 allow for further chemical analysis of the samples.

Just like with the Scanning Electron Microscope, the TEMs take advantage of the wave-particle duality of electrons, except that they rely more on the wave-like properties of the electrons for imaging. Another benefit of the use of the TEM is the resolution that arises from using accelerated electrons for imaging. Louis de

Broglie related a particle's momentum (p) to its wavelength (λ) though his well-known equation:

$$\lambda = \frac{h}{p} \tag{C.1}$$

where h is Plank's constant. For a electrons with energy higher than $100keV$, like it is the case with these TEMs, it should be the relativistic momentum the one to be used for equation C.1. This substitution yields

$$\lambda = \frac{h}{\left[2m_0eV\left(1 + \frac{eV}{2m_0c^2}\right)\right]^{\frac{1}{2}}} \tag{C.2}$$

where m_0 is the mass of the electron, c is the speed of light and eV is the energy of the accelerated electron. For a 300 kV electron, the associated wavelength using C.2 is 0.019 Å. Nonetheless, the achievable resolution is much lower due to lens aberration effects.

Imaging is obtained through the forward scattering of electrons through the sample. Furthermore, due to the electron-sample interactions that take place during the imaging process, it is possible to obtain a higher wealth of information regarding the specimen. Characteristic X-rays, visible light, Auger Electrons, Back-Scattered Electrons, and Secondary Electrons are among some of the interactions that take place during the TEM imaging process and can be collected trough the use of an analytic TEM. Though several signals are produced through these electron-sample interactions, this part of the study focuses on the imaging of the sample itself, and the use of electron diffraction as a tool for characterization. Despite the analytical abilities, and better resolution of the TF20, the TF30 is more than adequate to perform this initial study.

C.1.1 Imaging with the Transmission Electron Microscope

Akin to an optical microscope, the TEM is equipped with an illumination source, focussing lenses, a sample stage, and means of viewing the magnified image. The main differences being of course that it employs electrons instead of photons, the lenses being magnetic lenses. Figure C.1 shows a rough, and very simplified, schematic of the illumination and imaging system in the TEM. The figure also displays two of the modes commonly used to obtain information from the sample.

Part of the illumination system of the TEM consists of a Field Electron Gun (FEG). One of the advantages of this is the narrow energy spread of the electrons extracted from it. The lenses and aperture above the sample allow for the control of the probe used to illuminate the sample. This is necessary as different imaging conditions require different currents in order to obtain usable images. As illustrated in figure C.1 when the electrons from the beam interact with the specimen, they scatter and diffract. The objective lens serves to form both a diffraction plane and an image plane. Apertures may be placed in these planes in order to select what information can be collected from the specimen. For example, an aperture may be placed in the diffraction plane in order to only let one of the diffracted beams through, and thus image the sample with the electrons that satisfy that particular diffraction condition. Also, an aperture may be placed in the image plane and isolate a specific area of the sample from which to obtain diffraction information. The intermediate lens can then be used to select which of the two planes to use to create the final image. Finally the projector lens will project the final image onto a screen or recording medium.

Without any apertures used in the image or diffraction planes, the main beam, and all the diffracted beams will be used to create the final image. Since the path length traveled by all these beams is quite close to being the same, the resulting image is often low in contrast. Any contrast observed in such an image usually arises from mass
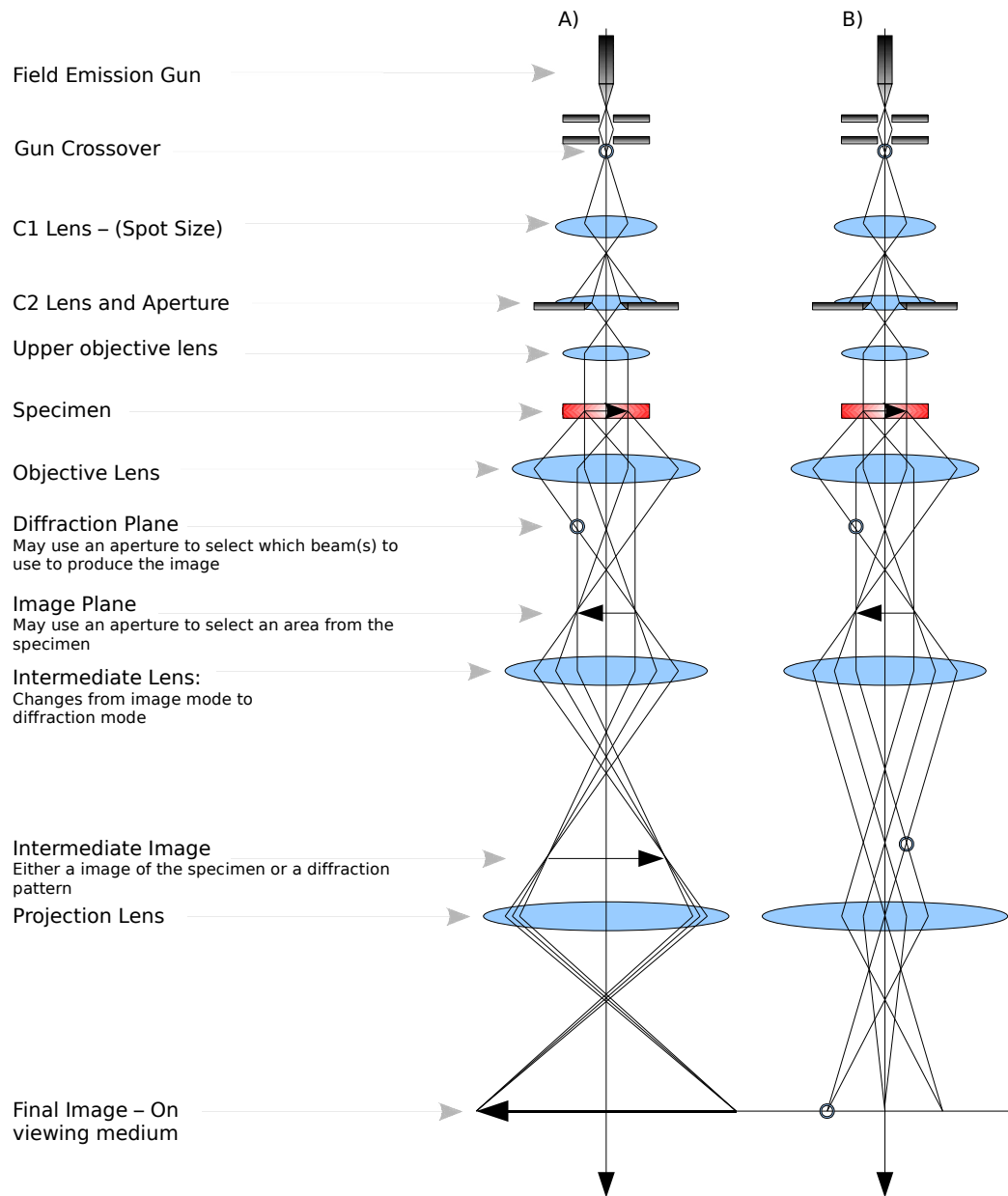
Figure C.1 Rough schematic of the TEM's illumination and imaging system as set for obtaining A) an image of the specimen or B) electron diffraction from the specimen

or thickness differences in the sample it self. Nonetheless, since electron diffraction information can be obtained from the specimen, there are two basic modes that allow for higher contrast while imaging the sample: Bright-Field, and Dark-Field. Under a bight-field image condition, an aperture is placed to select only the main beam that comes through the sample and block any other diffracted beams. Under a dark-field imaging condition, one of the diffracted beams is selected to form the image, while blocking the main beam. The bright and dark-field terms seem obvious as the main beam usually carries most of the electrons, thus selecting it or blocking it will yield images of different brightnesses.

TEM Sample Preparation: In order to be able to image the samples using the Transmission Electron Microscope, the sample must be thin enough to become "electron transparent." This means that the thickness of a good TEM sample is smaller than the mean-free path of the electrons. "Electron transparency" varies from material to material, and in TEM sample preparation thinner is better. Nevertheless, it is often the goal to achieve samples where there is a region thinner than 100 nm.

Plan-view (as well as cross-sectional) samples were prepared in order to characterize the VO_2 films with the Transmission Electron Microscope. Both sets of samples were prepared using the "wedge" technique. For a cross-sectional sample, the film is "sandwiched" together, and both sides of the sample polished, leaving a small, thin area of interest where the film may be observed. On the other hand, with plan-view samples, the film is left untouched while the substrate is polished from underneath in order to create a wedge. Figure C.2 shows the areas of interest for cross-sectional and plan view wedge samples after they have been thinned.

For both samples, the wedge is polished so that the angle in the wedge is approximately 1°, in that manner, the area that is 50 nm or thinner may extend close to
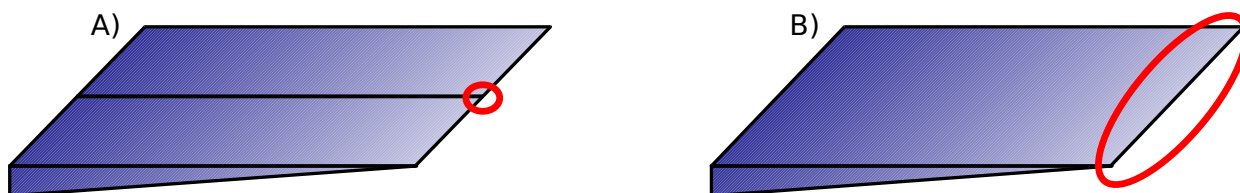
Figure C.2 TEM "wedge" samples for A) a cross-sectional view, where the film is "sandwiched" between two silicon pieces in order to view its thickness; and B) a plan-view where the substrate is polished thin leaving the film undisturbed along the edge

2.5 μm. This gives a substantial region of interest to analyze the film and particles. These wedges are finally secured to a 3 mm-diameter copper washer for support.

Note: Most of the sample preparation and imaging discussed in this chapter was carried out by Brady Cox and Michael Miller for their REU projects and Senior Thesis.

C.1.2 Beyond the Scanning Electron Microscope

The results obtained in the previous chapter were reported with grain sizes greater than 100 nm, and the technique applied worked better for particles greater than 300 nm. The reason was the need to have grains thick enough to allow Back-Scattered Electrons to obtain an indexable EBSD pattern. Further, due to the use of 20 kV accelerated electrons, the resolution limits of the instrument began to be evident at 100 kX magnification.

The Transmission Electron Microscope has the resolution and ability to image crystalline grains smaller that the limits found in the Scanning Electron Microscope. As mentioned before, the manufacturer of the TF30 specifies a resolution of 2.4 Å. Likewise, it also has ability to obtain structural information through the use of electron diffraction from those smaller grains. The ability to obtain higher resolution
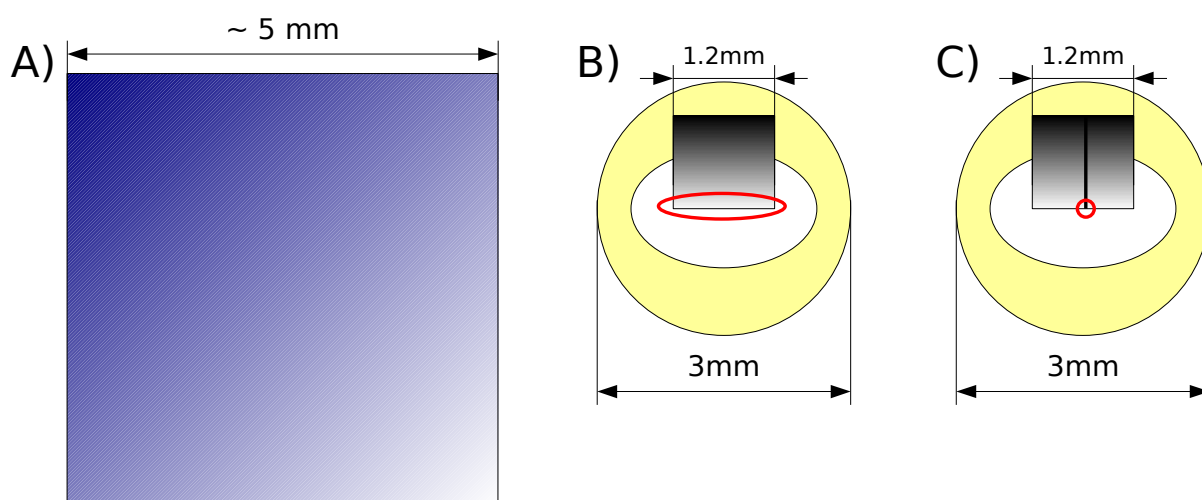
Figure C.3 Size comparison between A) a typical SEM sample used, and two TEM samples, B) a plan-view and C) a cross-sectional view. While the SEM can image the whole surface, the imageable area is greatly reduced in the TEM samples.

images allowed for the observation of crystallized vanadium dioxide grains in the sample annealed at 400°C for 17 hrs. In addition, the TF20 further has the ability to analyze the films at a scale that surpasses that of the SEM

However, this added information that can be obtained through the use of these TEMs comes at a price. As mentioned before, the samples need to be thinned down to be electron transparent, and they must fit inside a 3 *mm*-diameter support with an even smaller window. Figure C.3 shows a relative comparison of the sample sizes for the SEM and TEM, as well as their regions of interest. Despite the reduced imageable area in the TEM samples, it can be assumed that the data collected from a particular region is representative of the film as a whole.

C.1.3 Bright and Dark Field Characterization

Figure C.1a shows a ray diagram of the imaging process in the TEM. As it is observed from the diagram, the diffracted rays, as well as the main beam are all combined in

the final image. This often results in an image of little contrast due to the interference between the main beam and the diffracted beams. Under these conditions, any contrast that appears in the image is usually achieved due to variations in thickness or differences in mass in the sample. (This is commonly known as Mass-Thickness contrast as it is non-trivial to differentiate between the two.) Added contrast might be achieved while imaging by "blocking" or "selecting" the desired beams that will allow for the image to be formed. In this manner, the interference of the blocked beams is eliminated, and the image from the selected beam(s) is enhanced. This selection process is achieved by placing "apertures," (a thin sheet of metal with a hole drilled through it) that allow the user to "select" or "block" information to form the desired image. Some of these apertures are located in the diffraction plane and the image plane (see fig C.1) and these are varied in size.

A Bright-Field (BF) condition is created by using an aperture in the diffraction plane to select the main beam while blocking the diffracted beams.[1] Under these conditions, the main beam is used to create the image and contrast is enhanced since the interference of the diffracted beams is eliminated. Since the main beam carries most of the electrons the image looks bright (hence, Bright-Field). This seems to be a very common and one of the easiest ways to obtain images, specially since the sample needs not be crystalline.

On the other hand, a Dark-Field (DF) condition is created by using the aperture to block the main beam and instead selecting a diffracted beam to form the image.[2] In this case, the main beam (which carries most of the electrons) is blocked, and the image is formed only by those electrons that satisfy the Bragg condition necessary to

---

[1]Known as the Objective Aperture

[2]To get better images, it is preferred that the beam itself is tilted in such a way that the selected diffracted beam is placed where the main beam used to be. This allows for the aperture to remain in place, and for the rest of the optics to use a centered beam.

diffract to that chosen spot. Since most the electrons are blocked, the image tends to be darker (hence Dark-Field). However, intensity might be increased by tilting the sample in such a way that the selected diffraction spot shares a comparable amount of electrons to the main beam (a two-beam condition).

A Dark-Field imaging mode is peculiar as it forms an image only from those crystals in the sample that are aligned in such a way as to meet the required diffraction condition. As such, the image will show brightness in areas where the orientation of the crystals meets the specified diffraction condition.

C.2 Resistance Measurement Setup

In order to characterize the films by the use of electrical measurements, it is necessary to have electrical contacts to the film. The VO_2 films are 50 nm thick. Films this thin tend to be rather fragile to probes, as the contact with the probes might damage the film itself and measure the substrate instead. Thus, it is imperative to take care of how the electrical contacts are attached to the sample itself. It was imperative to find a material that will allow electrical measurements while being gentle on the film. A thin gold wire with the end melted into a ball seems an adequate contact. Gold is a soft metal with very good conductivity. Figure C.4 shows how the thin gold wire with a "gold-ball" at the end may be used as a contact while putting little pressure on the film.

Simple resistance measurements are carried out by the use of two probes and measuring the resistance across the film itself. Though resistivity measurements are better performed through the use of a 4-point probe setup (because of the elimination of contact resistance) a 2-point probe is adequate. These measurements will be used to observe the phase transition while measuring the resistance as opposed to the

Figure C.4 Picture of a characteristic gold probe used for electrical measurements. The wire itself is used to provide a "springy" contact of the ball to the film.

resistivity.

The resistance measurement takes place by the use of a simple voltage divider. The schematic diagram for the electronics used for this measurements can be found in figure C.5 where a resistor is used as a reference to calculate the film's resistance.
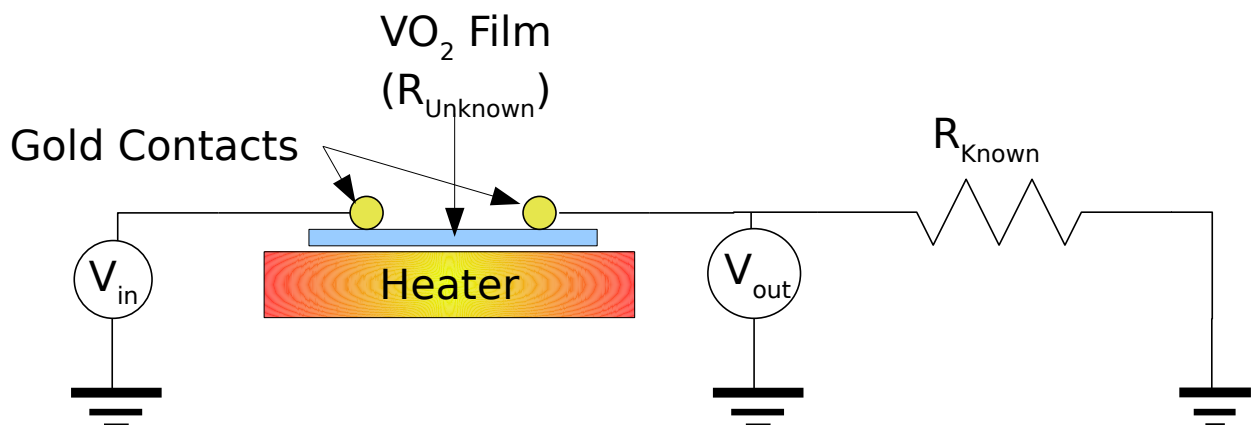

Figure C.5 Diagram showing how the film resistace was measured during the transition. A voltage divider circuit was set up with a reference resistance. The contacts to the film were gold balls mechanically in contact with the film.

The calculation of of the film resistance can be achieved by the use of Equation C.2

$$R_{Film} = R_{Known} \left(\frac{V_{in}}{V_{out}} - 1 \right) \tag{C.3}$$

Where R_{Film} is the resistance of the film, R_{Known} is the known resistance in the circuit, V_{in} is the voltage supplied, and V_{out} is the voltage measured.

Resistance measurements require a conductive path through the film. With this consideration, the resistance measurements have to be restricted to analyze only films where such conductive path may be found. This eliminates the samples where films of isolated particles were formed.

With the use of the "gold-ball" contacts resistance was measured across the films while the sample was heated up.[3] As mentioned in Section 1.1.2 the amorphous VO_X film does not show the sharp phase transition but rather the decrease in resistance, as temperature increases, that can be observed with semiconductors. However, the transition was observed for some of the crystalline thin films produced

---

[3]Temperature was monitored with a thermocouple while heating took place. In order to avoid stray readings from the thermocouple onto the electrical measurements, the temperature was taken at a separate silicon wafer. Using this technique, the measured error in temperature was +/- 1° Celsius

Bibliography

[1] F. J. Morin, "Oxides Which Show a Metal-to-Insulator Transition at the Neel Temperature," Phys. Rev. Lett. **3,** 34–36 (1959).

[2] M. M. Qazilbash, K. S. Burch, D Whisler, D. Shrekenhamer, B. G. Chae, H. T. Kim, and D. N. Basov, "Correlated metallic state of vanadium dioxide," Journal Name **1,** Pages (2006).

[3] A. Zylbersztejn and N. F. Mott, "Metal-insulator transition in vanadium dioxide," Phys. Rev. B **11,** 4383–4395 (1975).

[4] T. Maruyama and Y. Ikuta, "Vanadium dioxide thin films prepared by chemical vapour deposition from vanadium(III) acetylacetonate," Journal of Materials Science **28,** 5073–5078 (1993).

[5] H. W. Verleur, A. S. Barker, and C. N. Berglund, "Optical Properties of VO_2 between 0.25 and 5 eV," Phys. Rev. **172,** 788–798 (1968).

[6] S. Shin, S. Suga, M. Taniguchi, M. Fujisawa, H. Kanzaki, A. Fujimori, H. Daimon, Y. Ueda, K. Kosuge, and S. Kachi, "Vacuum-ultraviolet reflectance and photoemission study of the metal-insulator phase transitions in VO_2, V_6O_{13}, and V_2O_3," Phys. Rev. B **41,** 4993–5009 (1990).

[7] K. A. Khan and M. S. Rahman Khan, "Preparation and properties of vanadium dioxide thermochromic thin films," Pramana **38,** 389–396 (1992).

[8] Moon-Hee Lee and Jun-Seok Cho, "Better thermochromic glazing of windows with anti-reflection coating," Thin Solid Films **365,** 5–6 (2000).

[9] C. H. Koo, J. S. Lee, M. W. Kim, Y. J. Chang, T. W. Noh, J. H. J. B. G. Chae, and H. T. Kim, "Optical investigations on electronic structure changes related to the metal-insulator transition in VO_2 film,", 2005.

[10] Y. Dachuan, X. Niankan, Z. Jingyu, and Z. Xiulin, "Vanadium dioxide films with good electrical switching property," Journal of Physics D: Applied Physics **29,** 1051–1057 (1996).

[11] H. J. Schlag and W. Scherber, "New sputter process for VO_2 thin films and examination with MIS-elements and C-V-measurements," Thin Solid Films **366,** 38–31 (2000).

[12] C. Hébert, M. Willinger, D. S. Su, P. Pongratz, P. Schattschneider, and R. Schlögl, "Oxygen K-edge in vanadium oxides: simulations and experiments," European Physical Journal B **28,** 407–414 (2002).

[13] K. K. Sukeji Kachi, Tosio Takada, "Electrical Conductivity of Vanadium Oxides," Journal of the Physical Society of Japan **18,** 1839–1840 (1963).

[14] R. M. Wentzcovitch, W. W. Schulz, and P. B. Allen, "VO_2: Peierls or Mott-Hubbard? A view from band theory," Phys. Rev. Lett. **72,** 3389–3392 (1994).

[15] V. Eyert, "The metal-insulator transitions of VO_2: A band theoretical approach," Annalen der Physik **11,** 650–704 (2002).

[16] A. Liebsch, H. Ishida, and G. Bihlmayer, "Coulomb Correlations and Orbital Polarization in the Metal Insulator Transition of VO_2,", 2003.

[17] S. Biermann, A. Poteryaev, A. I. Lichtenstein, and A. Georges, "Dynamical Singlets and Correlation-Assisted Peierls Transition in VO_2," Physical Review Letters **94,** 026404–+ (2005).

[18] P. P. Boriskov, A. L. Pergament, A. A. Velichko, G. B. Stefanovich, and N. A. Kuldin, "Metal-insulator transition in electric field: A viewpoint from the switching effect,", 2006.

[19] K. Kosuge, S. Kachi, H. Nagasaki, and S. Minomura, "Phase Transition in V_6O_{13}," Journal of the Physical Society of Japan **20,** 178–+ (1965).

[20] H. K. Kosuge, K.; Okinaka, "Metal insulator phase transition and magnetic properties of V_nO_{2n-1}," IEEE Transactions on Magnetics **8,** 581–583 (1972).

[21] S. Horiuchi, M. Saeki, Y. Matsui, and F. Nagata, "Transition of V_6O_{13} to VO_2 observed with a high-resolution electron microscope," Acta Crystallographica Section A **31,** 660–664 (1975).

[22] "Inorganic Crystal Structure Database,".

[23] D. B. McWhan, M. Marezio, J. P. Remeika, and P. D. Dernier, "X-ray diffraction study of metallic VO_2," Phys. Rev. B **10,** 490–495 (1974).

[24] D. Watanabe, B. Andersson, J. Gjønnes, and O. Terasaki, "Determination of structure factors of disordered vanadium monoxide crystals by the intersecting-Kikuchi-line and critical-voltage methods," Acta Crystallographica Section A **30,** 772–776 (1974).

[25] D. Kucharczyk and T. Niklewski, "Accurate X-ray determination of the lattice parameters and the thermal expansion coefficients of VO_2 near the transition temperature," Journal of Applied Crystallography **12,** 370–373 (1979).

[26] R. Lopez, T. E. Haynes, L. A. Boatner, L. C. Feldman, and J. R. F. Haglund, "Size effects in the structural phase transition of VO_2 nanoparticles," Physical Review B. **65,** 1–5 (2002).

[27] Wang X.J, Li H.D., Fei Y.J., Wang X., Xiong Y.Y., Nie Y.X., and Feng K.A., "XRD and Raman study of vanadium oxide thin films deposited on fused silica substrates by RF magnetron sputtering," Applied Surface Science **177,** 8–14 (2001).

[28] B. J. Campbell, H. T. Stokes, D. E. Tanner, and D. M. Hatch, "ISODISPLACE: a web-based tool for exploring structural distortions," Journal of Applied Crystallography **39,** 607–614 (2006).

[29] R. M. B. J. M. Gregg, "The effect of applied strain on the resistance of VO_2 thin films," Applied Physics Letters **71,** 3649–3651 (1997).

[30] A. Cavalleri, T. Dekorsy, H. H. Chong, J. C. Kieffer, and R. W. Schoenlein, "Evidence for a Structurally-driven Insulator-to-metal Transition in VO_2: a View from the Ultrafast Timescale," Physical Review B **70,** 161102 (2004).

[31] R. Lopez, L. A. Boatner, T. E. Haynes, J. R. F. Haglund, and L. C. Feldman, "Enhanced hysteresis in the semiconductor-to-metal phase transition of VO_2 precipitates formed in SiO_2 by ion implantation," Applied Physics Letters **79,** 3161–3163 (2001).

[32] A. Cavalleri, C. Tóth, C. W. Siders, J. A. Squier, F. Ráksi, P. Forget, and J. C. Kieffer, "Femtosecond Structural Dynamics in VO_2 during an Ultrafast Solid-Solid Phase Transition," Phys. Rev. Lett. **87,** 237401 (2001).

[33] V. N. Mark Borek, F. Qian, "Pulsed laser deposition of oriented VO_2 thin films on R-cut sapphire substrates," Applied Physics Letters **63,** 3288–3290 (1993).

[34] B. G. Chae, D. H. Youn, H. T. Kim, S. Y. Maeng, and K. Y. Kang, "Fabrication and Electrical Properties of Pure VO_2 Phase Films," ArXiv Condensed Matter e-prints (2003).

[35] R. Lopez, L. A. Boatner, T. E. Haynes, L. C. Feldman, and J. R. F. Haglund, "Synthesis and characterization of size-controlled vanadium dioxide nanocrystals in a fused silica matrix," Journal of Applied Physics **92,** 4031–4036 (2002).

[36] A. G. Cullis and P. D. Augustus, *Microscopy of Semiconducting Materials, 1987: Proceedings of the Institute* (CRC Press, 1987).

[37] Yue Kuo, *Thin Film Transistors: Materials and Processes*, 1 ed. (Springer, 2003).

[38] Robert A. Street, *Technology and Applications of Amorphous Silicon* (Springer, 2000).

[39] D. B. Williams and B. C. Carter, *Transmission Electron Microscopy: a textbook for materials science* (Springer, 1996).

[40] EDAX, TSL, and AMETEK, "Introduction to OIM Analysis,", Training in PDF form, 2006.

[41] R. P. Goehner and J. R. Michael, "Phase Identification in a Scanning Electron Microscope Using Backscattered Electron Kikuchi Patterns," Journal of Research of the National Institute of Standards and Technology **101,** 301–308 (1996).

[42] J. K. Farrer, Ph.D. thesis, University of Minnesota, 2004.

[43] H. T. Stokes, D. M. Hatch, and B. J. Campbell, "ISOTROPY,", stokes.byu.edu/isotropy.html, 2007.

Index